

# Asymmetry effects in homodyne and heterodyne measurements: Positive operator-valued measures and asymptotic security of Gaussian continuous variable quantum key distribution

A. S. Naumchik,<sup>1,\*</sup> Roman K. Goncharov,<sup>1,†</sup> and Alexei D. Kiselev<sup>2,3,‡</sup>

<sup>1</sup>*ITMO University, Kronverksky Pr. 49, Saint Petersburg 197101, Russia*

<sup>2</sup>*Laboratory for Quantum Communications, ITMO University,*

*Birzhevaya Line, 16, Saint Petersburg 199034, Russia*

<sup>3</sup>*Laboratory of Quantum Processes and Measurements,*

*ITMO University, Kadetskaya Line 3b, Saint Petersburg 199034, Russia*

(Dated: December 30, 2025)

We use the Gaussian approximation describing photocount statistics for both the homodyne and the double homodyne (heterodyne) measurements to study asymmetry effects arising from imbalance of the beam splitters and variations in quantum efficiencies of the photodetectors. After computing the  $Q$  symbols of the positive operator-valued measures (POVMs) of noisy measurements that take into account the asymmetry effects, the operator representations for the POVMs are obtained in the form that assumes applying the additive noise quantum channel to the POVMs of noiseless (ideal) measurements. For double homodyne detection, it was found that the noiseless measurements should generally be expressed in terms of the projectors onto squeezed-states and the corresponding squeezed-state operator representation of POVM along with the measurement noise channel depend on the squeezing parameter that lies in the interval dictated by the condition for the excess noise covariance matrix to be positive semi-definite. The analytical results are used to perform analysis of the asymptotic security of the Gaussian-modulated continuous variable quantum key distribution (CV-QKD) protocol in the untrusted-noise scenario where the measurement noise is assumed to be accessible to an adversary. The inherent non-uniqueness of the operator representation for the double-homodyne POVM manifests itself in the squeezing dependent Holevo information that needs to be additionally optimized. For both types of the measurements, the mutual information, the Holevo information and the asymptotic secret fraction are sensitive to asymmetry effects leading to degraded performance of the protocol.

## I. INTRODUCTION

Optical homodyne detection is a well-established experimental technique of quantum optics for measuring phase-sensitive properties of light fields. In a typical four-port homodyne setup described in textbooks (see, e.g., the textbook [1]), a weak quantum signal is superimposed with a strong local oscillator (LO) at a beam splitter and the resulting output fields are detected with photodiodes, so that information about the properties of the signal field quadratures is extracted from the statistics of the difference photocurrent.

In the realm of continuous-variable (CV) quantum systems, this technique plays a key role of fundamentally important measurement method and, over the course of the last two decades of the past century, the homodyne-based measurement schemes have been the subject of numerous theoretical studies [2–14] reviewed in [15]. In the limit of strong local oscillator, the noiseless homodyne detection becomes a projective measurement described by projectors onto a suitable set of quadrature eigenstates, whereas similar result for the eight-port double homodyne scheme, which is known to be equivalent to the

so-called heterodyne detection scheme, is represented by the coherent states. In this case, homodyne and double homodyne (heterodyne) schemes can be regarded as implementations of Gaussian measurements defined as measurement procedures that produce a Gaussian probability distribution of outcomes for any Gaussian state [16, 17] (see also the monograph [18]). Note that the LO intensity and fluctuations induced effects emerging beyond the strong LO approximation are studied in Refs. [19–23].

A wide variety of technologically important applications, where the homodyne related techniques are of crucial importance, include the quantum tomography of CV states [24–35] and the quantum communication protocols [36, 37] such as the CV quantum teleportation [38, 39] and the continuous-variable quantum key distribution (CV-QKD) systems [40–43].

Practical security for real-world QKD systems requires the deviations between the system and the ideal to be assessed so as to take into account imperfections of devices [44, 45]. Imperfections of the photodetectors such as non-unity detector efficiencies, electronic noise, dark counts, finite bandwidth and photon-number resolution, detector dead times and afterpulses introduce excess noise that affects CV-QKD security [46–52]. Noisy homodyne and heterodyne measurements are no longer projective and has to be analyzed in terms of the positive operators-valued measures (POVMs). Imperfections

\* Email address: naumchik95@gmail.com

† Email address: toloroloe@gmail.com

‡ Email address: alexei.d.kiselev@gmail.com

leading to the measurement noise may open side channels exploitable by an adversary using either wavelength-dependent or detector-blinding attacks [53–56]. Countermeasures to such attacks include spectral filtering, detector balancing, and careful calibration of the photodetectors [57–59].

In this paper, we focus our attention on the quantum measurement imperfections that will be collectively referred to as the *asymmetry effects*. These effects arise from the unbalanced beam splitters and difference in quantum efficiencies of the photodetectors. Though in recent studies [60–62], the asymmetry effects are found to be of importance for quantum random number generators [60] and security analysis of CV-QKD [61, 62], a systematic POVM-based theoretical analysis has not yet been received proper attention. Our goal is to fill the gap. To this end, we derive the POVMs and study how the asymmetry effects influence the asymptotic security of the Gaussian CV-QKD protocol in the untrusted-noise scenario where an adversary controls measurement imperfections.

The paper is organized as follows. In Sec. II, we obtain the statistical distribution of difference photon counts with the asymmetry effects taken into account and apply the Gaussian approximation to deduce the  $Q$  symbol of the corresponding homodyne POVM. The general strategy described in Sec. II B is employed to deduce the operator representation for the POVM. In Sec. III, the eight-port double-homodyne scheme is analyzed using the method presented in the previous section. After deriving the  $Q$  symbol of POVM in the Gaussian approximation, we show that the operator representation of the POVM can be obtained by applying the additive noise channel with the squeezing dependent excess noise covariance matrix to the noiseless squeezed-state measurements. Thus, it turned out that the operator representation of the double-homodyne POVM is non-unique as it depends on the squeezing parameter. In Sec. IV, we apply our results for homodyne and double-homodyne detection to evaluate the asymptotic secret fraction for the Gaussian-modulated coherent-state CV-QKD protocol in the untrusted-noise scenario. It is found that, for heterodyne detection, the Holevo information requires additional optimization with respect to the squeezing parameter. Finally, in Sec. V, we summarize the main results and outline the directions for future research. Technical details are relegated to appendixes: Appendix A details analysis of the accuracy of the Gaussian approximation against the exact Skellam distributions; Appendix B examines alternative approximations using Bessel-function asymptotics of the Skellam distribution; Appendix C derives analytical expressions for mutual information under asymmetric detection and proves the equivalence between the preparation and measurement-based and entanglement-based protocol representations.

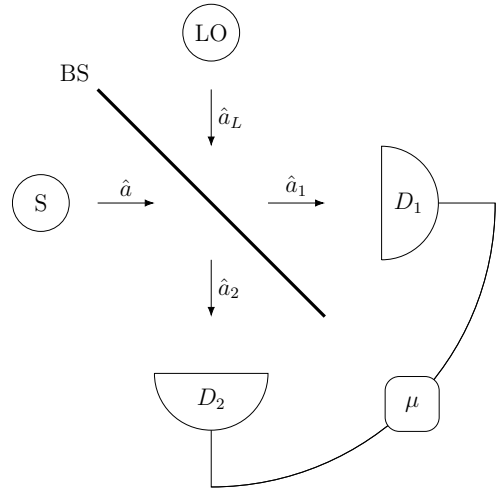


Figure 1: Scheme of a homodyne receiver:  $S$  is the source of the signal mode with the annihilation operator  $\hat{a}$ ,  $LO$  is the source of the reference mode (local oscillator) with the annihilation operator  $\hat{a}_L$ , and  $BS$  is the beam splitter with the amplitude transmission and reflection coefficients  $t = \cos \theta$  and  $r = \sin \theta$ , respectively; photodetectors  $D_1$  and  $D_2$  have quantum efficiencies  $\eta_1$  and  $\eta_2$ , and  $\mu \equiv m_1 - m_2$  is the photon count difference.

## II. HOMODYNE DETECTION

### A. Gaussian approximation

We begin with brief discussion of the homodyne measurement setup schematically depicted in Fig. 1. To this end, we assume that the beam splitter is unbalanced and its scattering matrix is chosen to be a real-valued rotation matrix with the transmission and reflection amplitudes,  $t$  and  $r$ , given by

$$t = \cos \theta \equiv C, \quad r = \sin \theta \equiv S. \quad (1)$$

Then the input coherent states of the signal mode and the local oscillator are transformed into the output coherent states as follows

$$|\alpha, \alpha_L\rangle \mapsto |\alpha_1, \alpha_2\rangle, \quad (2)$$

$$\alpha_1 = C\alpha + S\alpha_L, \quad \alpha_2 = -S\alpha + C\alpha_L, \quad (3)$$

so that the joint probability of  $m_1$  and  $m_2$  photon counts for the photodetectors  $D_1$  and  $D_2$  can be computed from the well-known Kelley-Kleiner formula [63] (see also Ref. [9]):

$$\begin{aligned} P(m_1, m_2) &= \langle \alpha_1, \alpha_2 | : \prod_{l=1}^2 \frac{(\eta_l \hat{n}_l)^{m_l} e^{-\eta_l \hat{n}_l}}{m_l!} : | \alpha_1, \alpha_2 \rangle \\ &= \prod_{l=1}^2 \frac{(\eta_l |\alpha_L|^2)^{m_l}}{m_l!} e^{-\eta_l |\alpha_L|^2} \end{aligned} \quad (4)$$

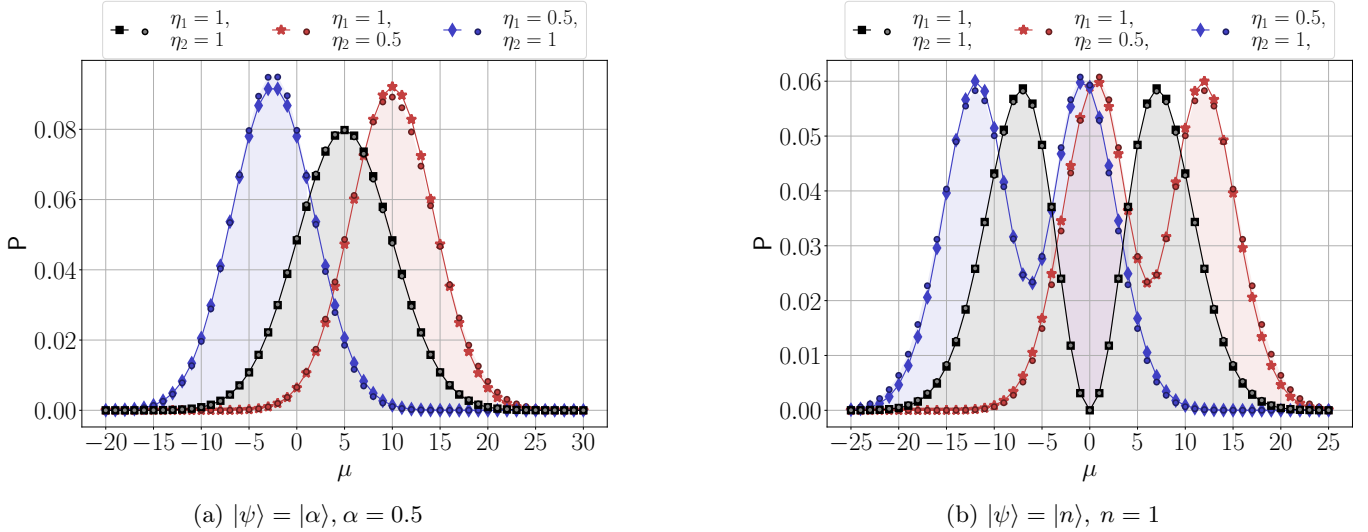


Figure 2: Exact (circle dots) and approximate (solid lines with markers) statistical distributions of photon count difference for the signal mode prepared in (a) the coherent state and in (b) the single photon Fock state computed for different efficiencies at  $|\alpha_L| = 5$  and balanced beam splitter.

where  $\dots$  stands for normal ordering, index  $l \in \{1, 2\}$  labels output ports of the beam splitter,  $\hat{n}_l = \hat{a}_l^\dagger \hat{a}_l$  is the photon number operator,  $m_l$  is the number of photon counts,  $\eta_l$  is the quantum efficiency of the detector  $D_l$ . We can now introduce the photon count difference

$$\mu = m_1 - m_2 \quad (5)$$

so that its statistical distribution can be written in the form of a product of the two Poisson distributions as follows

$$P(\mu) = \sum_{m_2=\max(0, -\mu)}^{\infty} \frac{(\eta_1 |\alpha_1|^2)^{\mu+m_2}}{(\mu+m_2)!} e^{-\eta_1 |\alpha_1|^2} \times \frac{(\eta_2 |\alpha_2|^2)^{m_2}}{m_2!} e^{-\eta_2 |\alpha_2|^2}. \quad (6)$$

It is well known that, by performing summation over  $m_2$ , the probability  $P(\mu)$  reduces to the Skellam distribution given by [64]

$$P(\mu) = e^{-\eta_1 |\alpha_1|^2} e^{-\eta_2 |\alpha_2|^2} \left( \frac{\eta_1 |\alpha_1|^2}{\eta_2 |\alpha_2|^2} \right)^{\mu/2} \times I_\mu \left( 2\sqrt{\eta_1 \eta_2 |\alpha_1|^2 |\alpha_2|^2} \right), \quad (7)$$

where  $I_k(z)$  is the modified Bessel function of the first kind [65].

An important point is that, at sufficiently large  $|\alpha_1|$  and  $|\alpha_2|$ , Poisson distributions that enter Eq. (4) can be approximated using the probability density functions of the normal distributions with mean and variance both equal to the mean of the corresponding Poisson distribution,  $\lambda_i = \eta_i |\alpha_i|^2$ . Then, in the continuum limit where summation in Eq. (6) is replaced with integration, the

Skellam distribution (7) can be approximated assuming that the amplitude of the local oscillator,  $|\alpha_L|$ , is large (the strong-LO approximation) and we can apply the convolution formula for Gaussian probability densities

$$\int G(x_1 - x_2; \sigma_1) G(x_2; \sigma_2) dx_2 = G(x_1; \sigma_1 + \sigma_2), \quad (8)$$

$$G(x; \sigma) \equiv \frac{1}{\sqrt{2\pi\sigma^2}} \exp\left(-\frac{x^2}{2\sigma^2}\right). \quad (9)$$

The above procedure immediately leads to the Gaussian approximation of the form:

$$P_G(\mu) = G(\mu - \mu_G; \sigma_G), \quad (10)$$

$$\sigma_G = \eta_1 |\alpha_1|^2 + \eta_2 |\alpha_2|^2 \approx (\eta_1 S^2 + \eta_2 C^2) |\alpha_L|^2, \quad (11)$$

$$\mu_G = \eta_1 |\alpha_1|^2 - \eta_2 |\alpha_2|^2 \approx (\eta_1 S^2 - \eta_2 C^2) |\alpha_L|^2 + CS(\eta_1 + \eta_2) |\alpha_L| \langle \hat{x}_\phi \rangle \quad (12)$$

where

$$\langle \hat{x}_\phi \rangle \equiv \langle \alpha | \hat{x}_\phi | \alpha \rangle = 2 \operatorname{Re} \alpha e^{-i\phi}, \quad \phi = \arg \alpha_L \quad (13)$$

is the average of the phase-rotated quadrature operator of the signal mode given by

$$\hat{x}_\phi = \hat{a} e^{-i\phi} + \hat{a}^\dagger e^{i\phi}. \quad (14)$$

Alternatively, the probability (10) can be rewritten in the form

$$P_G(x) \equiv P_G^{(H)}(x) = \frac{1}{\sqrt{2\pi\sigma_G^2}} \exp\left[-\frac{(x - \langle \hat{x}_\phi \rangle)^2}{2\sigma_x^2}\right], \quad (15)$$

where  $x$  is the quadrature variable given by

$$x \equiv \frac{\mu}{(\eta_1 + \eta_2) CS |\alpha_L|} - \frac{\eta_1 S^2 - \eta_2 C^2}{(\eta_1 + \eta_2) CS} |\alpha_L| \quad (16)$$

and  $\sigma_x$  is the quadrature variance

$$\sigma_x \equiv \frac{\eta_1 S^2 + \eta_2 C^2}{[(\eta_1 + \eta_2)CS]^2}. \quad (17)$$

Minimizing the variance (17) with respect to the transmittance  $C^2$  is straightforward:

$$\min_{C^2} \sigma_x = \left( \frac{\sqrt{\eta_1} + \sqrt{\eta_2}}{\eta_1 + \eta_2} \right)^2 \geq 1. \quad (18)$$

## B. Positive operator-valued measure

Our next step is to construct the positive operator-valued measure (POVM) based on the Gaussian approximation  $P_G$ . To this end, we note that the probability (15) is the expectation value of the POVM in the coherent state given by

$$P_G = \langle \alpha | \hat{\Pi}_G | \alpha \rangle. \quad (19)$$

The operator  $\hat{\Pi}_G$  can be regarded as a non-normalized density matrix describing a Gaussian state [18]. In the single mode case, such state is generally characterized by the  $2 \times 2$  covariance matrix  $\Sigma_m$  and the vector of averaged quadratures  $\mathbf{r}_m$ . So, the  $Q$  symbol of  $\Pi_G$  is determined by the Gaussian shaped distribution of the form:

$$\langle \alpha | \hat{\Pi}_G | \alpha \rangle \propto \exp\{-2(\mathbf{r} - \mathbf{r}_m)^T \times (\Sigma_m + \mathbb{1})^{-1}(\mathbf{r} - \mathbf{r}_m)\}, \quad (20)$$

$$\alpha = \alpha_1 + i\alpha_2, \quad \mathbf{r} = \begin{pmatrix} \alpha_1 \\ \alpha_2 \end{pmatrix}, \quad (21)$$

where  $\mathbb{1}$  is the identity matrix and the superscript  $T$  stands for transposition, so that the transpose of  $\mathbf{r}$  is the row vector:  $\mathbf{r}^T = (\alpha_1, \alpha_2)$ .

It is known that POVMs of noisy measurements can be introduced using the dual of a quantum channel acting on POVMs representing perfect (noiseless) measurements [18]. In what follows we shall use the classical mixing (additive noise) quantum channel

$$\Phi_N : \hat{\Pi}_{\text{id}} \mapsto \hat{\Pi}_G = \Phi_N(\hat{\Pi}_{\text{id}}) = \frac{2}{\pi\sqrt{\det \Sigma_N}} \times \int_{\mathbb{C}} d^2\beta \exp\{-2\mathbf{s}^T \Sigma_N^{-1} \mathbf{s}\} \hat{D}(\beta) \hat{\Pi}_{\text{id}} \hat{D}(-\beta), \quad (22)$$

where  $\mathbf{s}^T = (\text{Re}(\beta), \text{Im}(\beta)) = (\beta_1, \beta_2)$ ,  $d^2\beta = d\beta_1 d\beta_2$  and  $\hat{D}(\beta)$  is the displacement operator given by

$$\hat{D}(\beta) = e^{\beta\hat{a}^\dagger - \beta^*\hat{a}}. \quad (23)$$

This is a self-dual channel,  $\Phi_N^* = \Phi_N$ , that transforms the POVM of the ideal projective Gaussian measurements,  $\hat{\Pi}_{\text{id}}$ , into the POVM of the noisy measurements,  $\hat{\Pi}_G$ , by changing the covariance matrix  $\Sigma_{\text{id}}$  as follows

$$\Phi_N : \Sigma_{\text{id}} \mapsto \Sigma_G = \Sigma_{\text{id}} + \Sigma_N, \quad \Sigma_N \geq 0 \quad (24)$$

where  $\Sigma_N$  is the excess noise covariance matrix.

Our general strategy involves the following steps: (a) deriving the covariance matrix  $\Sigma_m$  from the  $Q$  symbol of POVM; (b) identifying the states representing ideal measurements and  $\Sigma_{\text{id}}$ ; and (c) constructing the POVM of the noisy measurements using the additive noise channel with the excess noise covariance matrix  $\Sigma_N = \Sigma_m - \Sigma_{\text{id}}$ .

In the case of the perfectly symmetric noiseless homodyne measurement with  $\eta_1 = \eta_2 = 1$  and  $C = S = 1/\sqrt{2}$ , the average (19) takes the form

$$\mathbb{P}_{\text{id}}^{(\text{H})} = \frac{1}{|\alpha_L|} Q_{x,\phi}(\alpha), \quad (25)$$

where  $x = \mu/|\alpha_L|$  and  $Q_{x,\phi}(\alpha)$  is the Husimi  $Q$  distribution for the eigenstate of the phase-rotated quadrature operator (14),  $|x, \phi\rangle$ , given by (see, e.g., the textbook [1])

$$Q_{x,\phi}(\alpha) = |\langle \alpha | x, \phi \rangle|^2 = G(x - \langle \hat{x} \rangle_\phi; 1). \quad (26)$$

Thus, we are led to the well-known result that, in the Gaussian approximation, the POVM describing sharp homodyne measurements

$$\hat{\Pi}_{\text{id}}^{(\text{H})} = \frac{1}{|\alpha_L|} |x, \phi\rangle \langle x, \phi| \quad (27)$$

is proportional to the projector onto  $|x, \phi\rangle$ .

Since the eigenstate of the rotated quadrature  $\hat{x}_\phi$  can be represented as the squeezed coherent state taken in the limit of infinitely large squeezing

$$|x, \phi\rangle = \hat{R}(\phi)|x\rangle, \quad \hat{R}(\phi) = \exp\{i\phi\hat{a}^\dagger \hat{a}\}, \quad (28)$$

$$|x\rangle = \lim_{r \rightarrow +\infty} \sqrt{\frac{\cosh(r)}{(2\pi)^{1/2}}} \hat{D}(x/2) \hat{S}(-r) |0\rangle, \quad (29)$$

where  $\hat{S}(r)$  is the squeezing operator given by

$$\hat{S}(\zeta) = e^{\frac{1}{2}(\zeta\hat{a}^{\dagger 2} - \zeta^*\hat{a}^2)}, \quad (30)$$

its covariance matrix assumes similar form [18]:

$$\Sigma_{\text{id}}^{(\text{H})} = \lim_{r \rightarrow +\infty} R(\phi) \text{diag}(e^{-2r}, e^{2r}) R^T(\phi), \quad (31)$$

where  $R_\phi$  is the rotation matrix given by

$$R(\phi) = \begin{pmatrix} \cos \phi & -\sin \phi \\ \sin \phi & \cos \phi \end{pmatrix}. \quad (32)$$

In a more general asymmetric case with  $\eta_1 \neq \eta_2$  and  $C \neq S$ , from the  $Q$  symbol (15) we deduce the following expression for the covariance matrix of noisy homodyne measurements

$$\begin{aligned} \Sigma_m^{(\text{H})} &= \lim_{r \rightarrow +\infty} R(\phi) \text{diag}(e^{-2r} + \sigma_N, e^{2r}) R^T(\phi) \\ &= \Sigma_{\text{id}}^{(\text{H})} + \Sigma_N^{(\text{H})}, \end{aligned} \quad (33)$$

$$\Sigma_N^{(\text{H})} = R(\phi) \text{diag}(\sigma_N, 0) R^T(\phi), \quad (34)$$

where  $\sigma_N$  is the excess noise given by

$$\sigma_N = \sigma_x - 1 \geq 0. \quad (35)$$

Note that the excess noise variance  $\sigma_N$  takes into account asymmetry effects and its non-negativity is guaranteed by inequality (18).

We can now use formula (22) along with the algebraic identities

$$\begin{aligned} & \int_{\mathbb{C}} d^2\beta \exp\{-2\mathbf{s}^T [R(\phi)\Sigma_N^{-1}R^T(\phi)]\mathbf{s}\} \hat{D}(\beta)\hat{\Pi}_{\text{id}}\hat{D}(-\beta) \\ &= \int_{\mathbb{C}} d^2\beta \exp\{-2\mathbf{s}^T \Sigma_N^{-1}\mathbf{s}\} \hat{D}(\beta e^{i\phi})\hat{\Pi}_{\text{id}}\hat{D}(-\beta e^{i\phi}), \end{aligned} \quad (36)$$

$$\hat{D}(\beta e^{i\phi})\hat{R}(\phi)\hat{D}(\alpha_m) = \hat{R}(\phi)\hat{D}(\beta)\hat{D}(\alpha_m) \quad (37)$$

to derive the POVM in the form of randomly displaced projectors

$$\begin{aligned} \hat{\Pi}_G^{(\text{H})} &= \frac{1}{(\eta_1 + \eta_2)CS|\alpha_L|} \\ &\times \int dx' G(x - x'; \sigma_N) |x', \phi\rangle\langle x', \phi|. \end{aligned} \quad (38)$$

Alternatively, this result can be obtained using the convolution identity (8) that leads to the relation

$$P_G^{(\text{H})}(x) = \sqrt{\frac{\sigma_x}{\sigma_G}} \int dx' G(x - x'; \sigma_N) Q_{x', \phi}(\alpha) \quad (39)$$

linking the Q symbols of the projectors  $|x', \phi\rangle\langle x', \phi|$  and the POVM  $\hat{\Pi}_G^{(\text{H})}$ .

The exact and approximate analytical results for photon count difference statistical distributions, given by Eq. (7) and Eq. (10) respectively, are valid for the case where the LO and signal modes are both in the coherent states. In the more general case when the quantum state of the signal mode is  $|\psi\rangle$ , the probability distributions can be evaluated using the relations

$$\begin{aligned} P(\mu; |\psi\rangle) &= \int P_{|\psi\rangle}(\alpha) P(\mu; \alpha) d^2\alpha, \\ P_G(x; |\psi\rangle) &= \langle \psi | \hat{\Pi}_G | \psi \rangle, \end{aligned} \quad (40)$$

where  $P_{|\psi\rangle}(\alpha)$  is the Glauber  $P$  function of the quantum state  $|\psi\rangle$ . In Fig. 2, we show the results computed for the single-photon Fock state obtained utilizing the well-known expression for the  $P$ -function of Fock states  $|\psi\rangle = |n\rangle$  given by

$$P_{|n\rangle}(\alpha) = \frac{e^{|\alpha|^2}}{n!} \left( \frac{\partial^2}{\partial \alpha \partial \alpha^*} \right)^n \delta^2(\alpha), \quad (41)$$

where  $\delta^2(\alpha) = \delta(\text{Re } \alpha)\delta(\text{Im } \alpha)$ .

Figure 2 displays the photocount difference probabilities computed from the exact and Gaussian probability distributions for the balanced beam splitter at different photodetector efficiencies and signal mode input states.

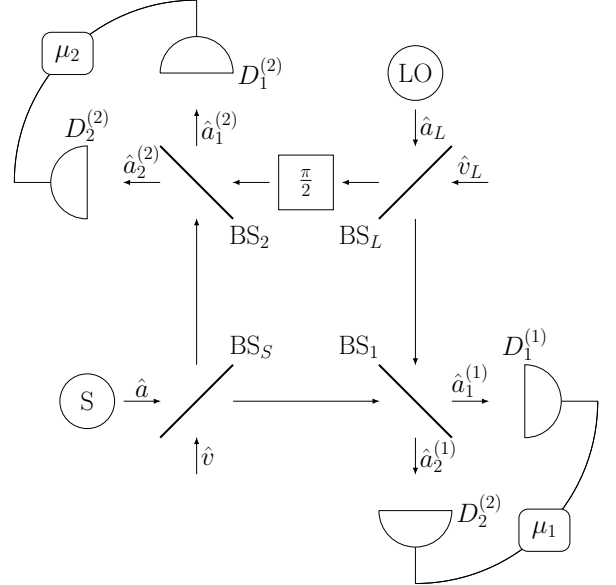


Figure 3: Scheme of an eight port double homodyne receiver. S is the source of the signal mode  $\hat{a}$ ; LO is the source of the reference mode  $\hat{a}_L$ ;  $BS_S$  ( $BS_L$ ) is the signal mode (local oscillator) beam splitter;  $\frac{\pi}{2}$  is the quarter wave phase shifter;  $BS_i$  is the beam splitter of  $i$ th homodyne;  $D_{1,2}^{(i)}$  are the photodetectors of the  $i$ th homodyne; and  $\mu_i = m_1^{(i)} - m_2^{(i)}$  is the photon count difference registered by the detectors of  $i$ th homodyne.

Fig. 2a shows that, in agreement with Eq. (12), asymmetry in photodetection results in the shift of the probability maximum.

The distributions for the single-photon states are depicted in Fig. 2b and, similar to the coherent state, demonstrate the effect of asymmetry-induced shift. Another noticeable effect is that the probability minimum between the central and side peaks become less pronounced.

From Fig. 2 it becomes apparent that performance of Gaussian approximation worsens in presence of asymmetry, which we will quantify in Appendix A.

Our concluding remark concerns an alternative method to approximate Eq. (7) with a Gaussian-shaped distribution which is based on the asymptotic expansions of the modified Bessel functions. In Appendix B we show that, for the asymmetric homodyne scheme, this method generally leads to ill-posed POVMs because the corresponding quadrature variance appears to be too small leading to negative contribution of the excess noise.

### III. DOUBLE HOMODYNE DETECTION

In this section, we consider the eight-port double homodyne scheme depicted in Fig. 3 (see, e.g., Refs. [1, 66]). This measurement scheme is known to allow reconstructing the Husimi  $Q$  function of the signal state [67] pro-

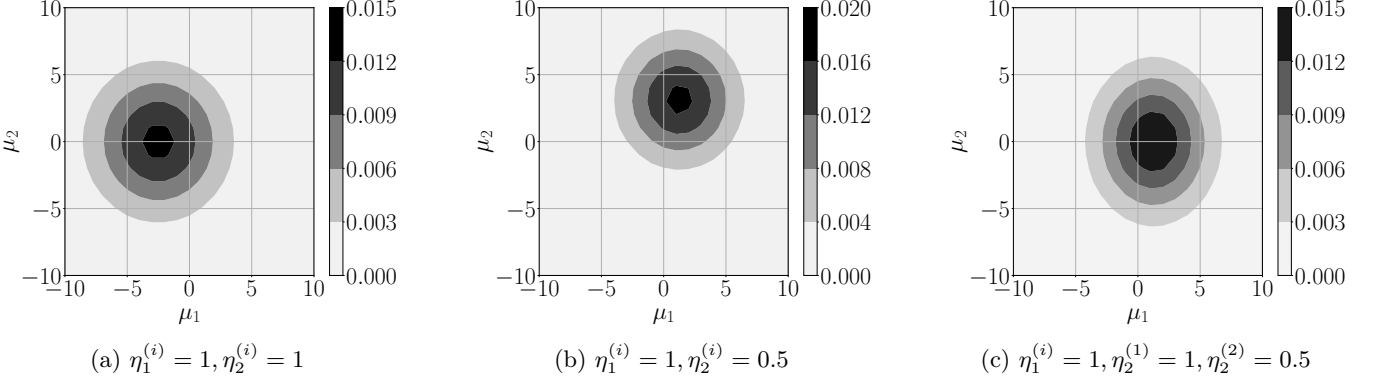


Figure 4: Double homodyne statistical distribution of photocount differences computed from Eq. (43) for various detector efficiencies at  $\alpha = 0.5$  and  $\alpha_L = 5$ . All the beam splitters are taken to be balanced.

viding complete information about the signal state that may be used in CV-QKD protocols. It should be noted that restoration of the complex amplitude of the state completely serves as the basis for composable security proofs [68, 69].

Figure 3 shows two homodyne setups with elements such as beam splitters  $BS_i$  and photodetectors  $D_{1,2}^{(i)}$  labeled by the index  $i \in \{1, 2\}$ . Referring to Fig. 3, the LO and signal modes are transmitted through the beam splitters  $BS_L$  and  $BS_S$ , respectively. Similar to the analysis performed in the previous section, we assume that the modes are in the coherent states,  $|\alpha\rangle$  and  $|\alpha_L\rangle$ . So, we have the amplitudes

$$\begin{aligned} \alpha^{(1)} &= C_S \alpha, & \alpha^{(2)} &= S_S \alpha, \\ \alpha_L^{(1)} &= C_L \alpha_L, & \alpha_L^{(2)} &= -i S_L \alpha_L, \end{aligned} \quad (42)$$

where  $\alpha^{(i)}$  ( $\alpha_L^{(i)}$ ) stands for the amplitude describing the input coherent state of the signal (LO) mode of the homodyne labeled by the upper index  $i \in \{1, 2\}$ . Note that the phase factor  $-i = e^{-i\pi/2}$  in the expression for  $\alpha_L^{(2)}$  is introduced by a suitably chosen phase shifter placed before the corresponding input port of the beam splitter  $BS_2$ .

Direct calculation shows that the joint statistics of the difference photocount events is determined by the product of the Skellam distributions given by

$$P(\mu_1, \mu_2) = P_1(\mu_1)P_2(\mu_2), \quad \mu_i = m_1^{(i)} - m_2^{(i)}, \quad (43)$$

$$\begin{aligned} P_i(\mu_i) &= e^{-\eta_1^{(i)}|\alpha_1^{(i)}|^2} e^{-\eta_2^{(i)}|\alpha_2^{(i)}|^2} \left( \frac{\eta_1^{(i)}|\alpha_1^{(i)}|^2}{\eta_2^{(i)}|\alpha_2^{(i)}|^2} \right)^{\mu_i/2} \\ &\times I_{\mu_i} \left( 2\sqrt{\eta_1^{(i)}\eta_2^{(i)}|\alpha_1^{(i)}|^2|\alpha_2^{(i)}|^2} \right), \end{aligned} \quad (44)$$

where, similar to the homodyne scheme, the amplitudes of the coherent states at the output ports of the beam splitter  $BS_i$

$$\alpha_1^{(i)} = C_i \alpha^{(i)} + S_i \alpha_L^{(i)}, \quad \alpha_2^{(i)} = -S_i \alpha^{(i)} + C_i \alpha_L^{(i)} \quad (45)$$

are expressed in terms of the transmission and reflection amplitudes,  $C_i = \cos \theta_i$  and  $S_i = \sin \theta_i$ .

We can now apply Eqs. (10)-(12) to approximate each Skellam distribution on the right hand side of Eq. (43) and derive the Gaussian approximation for the double homodyne scheme in the form:

$$P_G(\mu_1, \mu_2) = G(\mu_1 - \mu_G^{(1)}; \sigma_G^{(1)})G(\mu_2 - \mu_G^{(2)}; \sigma_G^{(2)}), \quad (46)$$

$$\sigma_G^{(i)} = (\eta_1^{(i)} S_i^2 + \eta_2^{(i)} C_i^2) |\alpha_L^{(i)}|^2, \quad (47)$$

$$\begin{aligned} \mu_G^{(i)} &= (\eta_1^{(i)} S_i^2 - \eta_2^{(i)} C_i^2) |\alpha_L^{(i)}|^2 + C_i S_i (\eta_1^{(i)} + \eta_2^{(i)}) |\alpha_L^{(i)}| \\ &\times 2 \operatorname{Re} \alpha^{(i)} e^{-i\phi}, \quad \phi = \arg \alpha_L. \end{aligned} \quad (48)$$

Similar to Eq. (15), it is useful to put the probability (46) into the following quadrature form:

$$\begin{aligned} P_G(x_1, x_2) \equiv P_G^{(\text{DH})}(x_1, x_2) &\equiv \frac{1}{2\pi\sqrt{\sigma_G^{(1)}\sigma_G^{(2)}}} \\ &\times \exp \left[ -\frac{(x_1 - \operatorname{Re} \alpha e^{-i\phi})^2}{\sigma_1^2} - \frac{(x_2 - \operatorname{Im} \alpha e^{-i\phi})^2}{\sigma_2^2} \right] \end{aligned} \quad (49)$$

where  $x_i$  are the quadrature variables given by

$$\begin{aligned} x_1 &= \frac{1}{2(\eta_1^{(1)} + \eta_2^{(1)}) C_1 S_1 C_S} \\ &\times \left\{ \frac{\mu_1}{|\alpha_L^{(1)}|} - (\eta_1^{(1)} S_1^2 - \eta_2^{(1)} C_1^2) |\alpha_L^{(1)}| \right\}, \end{aligned} \quad (50)$$

$$\begin{aligned} x_2 &= \frac{1}{2(\eta_1^{(2)} + \eta_2^{(2)}) C_2 S_2 S_S} \\ &\times \left\{ \frac{\mu_2}{|\alpha_L^{(2)}|} - (\eta_1^{(2)} S_2^2 - \eta_2^{(2)} C_2^2) |\alpha_L^{(2)}| \right\}, \end{aligned} \quad (51)$$

and relations

$$\sigma_1 = \frac{\sigma_x^{(1)}}{2C_S^2}, \quad \sigma_2 = \frac{\sigma_x^{(2)}}{2S_S^2}, \quad (52)$$

$$\sigma_x^{(i)} = \frac{\eta_1^{(i)} S_i^2 + \eta_2^{(i)} C_i^2}{[(\eta_1^{(i)} + \eta_2^{(i)}) C_i S_i]^2} \quad (53)$$

give the quadrature variances  $\sigma_1$  and  $\sigma_2$ .

As in Sec. II, formula (49) giving the  $Q$  symbol of POVM (see Eq. (19)) provides the starting point for reconstruction of the POVM describing the double homodyne measurements. The covariance matrix of the POVM reads

$$\Sigma_m^{(\text{DH})} = R(\phi) \text{diag}(\delta_1, \delta_2) R^T(\phi), \quad (54)$$

$$\delta_i = 2\sigma_i - 1, \quad (55)$$

whereas the column vector of the averaged quadratures is given by

$$\mathbf{r}_m^{(\text{DH})} = R(\phi) \begin{pmatrix} x_1 \\ x_2 \end{pmatrix}. \quad (56)$$

In the case, where all the beam splitters are balanced and the photodetection is perfect, we have

$$\begin{aligned} P_{\text{CS}}^{(\text{DH})}(x_1, x_2) &= \frac{|\langle \alpha | z e^{i\phi} \rangle|^2}{\pi |\alpha_L|^2}, \\ |\langle \alpha | z e^{i\phi} \rangle|^2 &= e^{-|z e^{i\phi} - \alpha|^2}, \quad z = x_1 + i x_2, \end{aligned} \quad (57)$$

so that the POVM is proportional to the projector onto the coherent state  $\hat{R}(\phi)|z\rangle = |(x_1 + i x_2) e^{i\phi}\rangle$ :

$$\hat{\Pi}_{\text{CS}}^{(\text{DH})}(x_1, x_2) = \frac{1}{\pi |\alpha_L|^2} |z e^{i\phi}\rangle \langle z e^{i\phi}|, \quad (58)$$

with the coherent state covariance matrix

$$\Sigma_{\text{CS}} = \mathbb{1} \quad (59)$$

equal to the identity matrix.

For nonideal measurements, following the steps of the general procedure described in Sec. II B, we need to identify the projectors representing the ideal measurements. At this stage, it is natural to assume these projectors are given by the coherent state projectors  $|z e^{i\phi}\rangle \langle z e^{i\phi}|$ . So, the covariance matrix of the additive noise quantum channel (22) is given by

$$\begin{aligned} \tilde{\Sigma}_N^{(\text{DH})} &= \Sigma_m^{(\text{DH})} - \Sigma_{\text{CS}} \\ &= 4R(\phi) \text{diag}(\tilde{\sigma}_N^{(1)}, \tilde{\sigma}_N^{(2)}) R^T(\phi), \end{aligned} \quad (60)$$

$$4\tilde{\sigma}_N^{(i)} = \delta_i - 1 = 2(\sigma_i - 1). \quad (61)$$

It is not difficult to check with the help of the convolution relation (8) that the probability (49) can be expressed as a Gaussian superposition of the coherent state Husimi functions

$$\begin{aligned} P_G^{(\text{DH})}(x_1, x_2) &= \frac{\sqrt{\sigma_1 \sigma_2}}{2\pi \sqrt{\sigma_G^{(1)} \sigma_G^{(2)}}} \int d^2\beta G(x_1 - \beta_1; \tilde{\sigma}_N^{(1)}) \\ &\quad \times G(x_2 - \beta_2; \tilde{\sigma}_N^{(2)}) |\langle \beta e^{i\phi} | \alpha \rangle|^2, \end{aligned} \quad (62)$$

where  $\beta = \beta_1 + i\beta_2$ , and  $\sigma_N^{(i)}$  is the excess noise variance given by Eq. (61). The corresponding expression for the

POVM reads

$$\begin{aligned} \hat{\Pi}_G^{(\text{DH})}(x_1, x_2) &= \frac{\sqrt{\sigma_1 \sigma_2}}{2\pi \sqrt{\sigma_G^{(1)} \sigma_G^{(2)}}} \int d^2\beta G(x_1 - \beta_1; \tilde{\sigma}_N^{(1)}) \\ &\quad \times G(x_2 - \beta_2; \tilde{\sigma}_N^{(2)}) |\beta e^{i\phi}\rangle \langle \beta e^{i\phi}|. \end{aligned} \quad (63)$$

An important point is that the results given by Eq. (62) and Eq. (63) are well defined only if the excess noise covariance matrix (60) is positive semi-definite:  $\tilde{\Sigma}_N^{(\text{DH})} \geq 0$ . The latter requires the variances  $\tilde{\sigma}_N^{(1)}$  and  $\tilde{\sigma}_N^{(2)}$  to be non-negative, which is equivalent to the inequalities:  $\sigma_1 \geq 1$  and  $\sigma_2 \geq 1$  (see Eq. (61)). From Eq. (52), we arrive at the conditions  $\sigma_x^{(1)} \geq 2C_S^2$  and  $\sigma_x^{(2)} \geq 2S_S^2$  be met.

When the beam splitter  $\text{BS}_S$  is balanced  $2C_S^2 = 2S_S^2 = 1$ , applicability of the above expression for the POVM is guaranteed by the inequality (see Eq. (18))

$$\sigma_x^{(i)} \geq \left( \frac{\sqrt{\eta_1^{(i)}} + \sqrt{\eta_2^{(i)}}}{\eta_1^{(i)} + \eta_2^{(i)}} \right)^2 \geq 1. \quad (64)$$

Otherwise, either  $2C_S^2$  or  $2S_S^2$  will be above unity, and the coherent-state representation is valid only if the value of the corresponding variance  $\sigma_x^{(i)}$  is sufficiently high. For example, at  $\eta_{1,2}^{(i)} = \eta < 1/2$ , the minimal values of  $\sigma_x^{(i)}$  are higher than 2 (see Eq. (64)) and the noise variance will be positive at any imbalance of the signal mode beam splitter because  $\max\{2C_S^2, 2S_S^2\} \leq 2$ .

When one of the noise variances (61) is negative, the POVM reconstruction procedure needs to be generalized. We shall present details on this generalization in the next section. Meanwhile, in the concluding part of this section, we confine ourselves to the cases where  $\sigma_N^{(i)}$  are positive.

The effects of photodetection asymmetry are illustrated in Fig. 4 which presents numerical results for the double homodyne distribution (43) in the photocount difference  $\mu_1 - \mu_2$  plane. Referring to Fig. 4, in addition to the shift of the distribution, the asymmetry induced difference of the variances at  $\eta_1^{(1)} + \eta_2^{(1)} \neq \eta_1^{(2)} + \eta_2^{(2)}$  manifests itself as the two dimensional anisotropy of the double homodyne distribution.

### A. Positive operator-valued measure and squeezed states

In this section we apply our general procedure outlined in Sec. II B to double homodyne measurements so as to derive the POVM expressed in terms of the projectors describing sharp (ideal) measurements. According to the previous section, the class of such measurement states, which are assumed to be Gaussian, should be extended beyond the family of the coherent states even though these states represent the measurements in the limiting case of balanced beam splitters and perfect photodetection. So, we begin with the generalized representation

of noiseless measurements that uses a set of pure states enlarged so as to include the squeezed states taken in the form

$$|z, r, \phi\rangle = \hat{R}(\phi)\hat{D}(z)\hat{S}(r)|0\rangle = \hat{D}(ze^{i\phi})\hat{S}(re^{2i\phi})|0\rangle, \quad (65)$$

where  $\hat{D}(\beta)$  ( $\hat{S}(\zeta)$ ) is the displacement (squeezing) operator given by Eq. (23) (Eq. (30)).

Then the covariance matrix of the noiseless POVM proportional to the projectors  $|z, r, \phi\rangle\langle z, r, \phi|$  is given by

$$\Sigma_{\text{id}}^{(\text{DH})} = R(\phi) \begin{pmatrix} e^{2r} & 0 \\ 0 & e^{-2r} \end{pmatrix} R^T(\phi), \quad (66)$$

whereas formula (56) giving the vector of the averaged quadratures remains applicable to the case of the squeezed states. As a result, the non-normalized Husimi distribution for the squeezed state (65) takes the form

$$\begin{aligned} |\langle ze^{i\phi}, re^{2i\phi} | \alpha \rangle|^2 &= \frac{1}{\cosh r} \exp \left[ -\frac{2}{e^{2r} + 1} (x_1 - \tilde{\alpha}_1)^2 \right. \\ &\quad \left. - \frac{2}{e^{-2r} + 1} (x_2 - \tilde{\alpha}_2)^2 \right], \end{aligned} \quad (67)$$

$$\tilde{\alpha}_1 = \text{Re } \alpha e^{-i\phi}, \quad \tilde{\alpha}_2 = \text{Im } \alpha e^{-i\phi}. \quad (68)$$

From Eqs. (54) and (66), we derive the covariance matrix of the additive noise channel

$$\begin{aligned} \Sigma_N^{(\text{DH})}(r) &= \Sigma_m^{(\text{DH})} - \Sigma_{\text{id}}^{(\text{DH})} \\ &= R(\phi) \begin{pmatrix} 4\sigma_N^{(1)}(r) & 0 \\ 0 & 4\sigma_N^{(2)}(r) \end{pmatrix} R^T(\phi) \geq 0, \end{aligned} \quad (69)$$

where

$$4\sigma_N^{(1)}(r) = \delta_1 - e^{2r}, \quad 4\sigma_N^{(2)}(r) = \delta_2 - e^{-2r}. \quad (70)$$

Since this matrix should be positive semi-definite, the noise variances (70) cannot take negative values.

For subsequent analysis, it will be useful to express the covariance matrix elements  $\delta_i$  given by Eq. (55) in terms of the imbalance (reflection-to-transmission) ratio of the input beam splitter,  $q$ , and the parameters  $\sigma_x^{(1)}$  and  $\sigma_x^{(2)}$  (see Eq. (53)):

$$\delta_1 \equiv 2\sigma_1 - 1 = (q + 1)\sigma_x^{(1)} - 1 \geq q = \frac{S_S^2}{C_S^2}, \quad (71a)$$

$$\delta_2 \equiv 2\sigma_2 - 1 = (q^{-1} + 1)\sigma_x^{(2)} - 1 \geq q^{-1} = \frac{C_S^2}{S_S^2}, \quad (71b)$$

where we used the fact that  $\sigma_x^{(i)} \geq 1$  (see Eq. (64)).

We assume without the loss of generality that the reflectance of the input beam splitter  $\text{BS}_S$  is larger than its transmittance, so that the imbalance ratio is above unity

$$q = \frac{1 - C_S^2}{C_S^2} = \frac{S_S^2}{C_S^2} \geq 1. \quad (72)$$

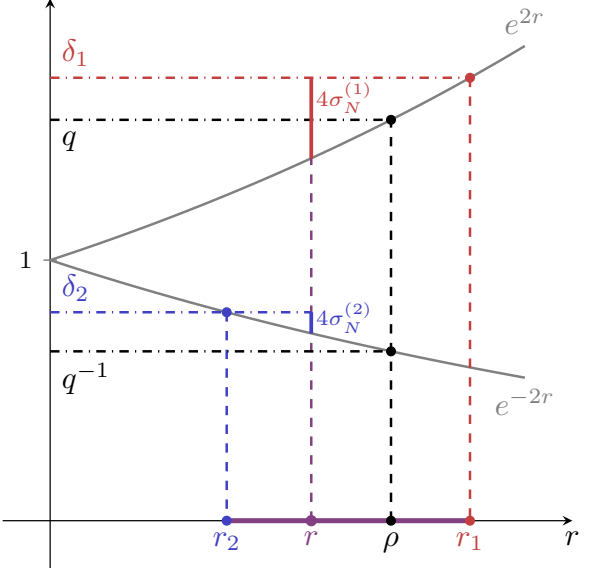


Figure 5: Geometry in the  $\delta$ - $r$  (principal variance-squeezing parameter) plane. Noise variances (70) are positive when the principal variance  $\delta_1$  ( $\delta_2$ ) is above  $e^{2r}$  ( $e^{-2r}$ ), so that the squeezing parameter  $r$  is ranged between  $r_1$  and  $r_2$ . Solid grey lines represent the graphs of the exponents:  $e^{2r}$  and  $e^{-2r}$ . In the case, where  $\delta_1 = q$  and  $\delta_2 = q^{-1}$ , the interval is reduced to the point  $r_1 = r_2 = \rho$ .

As is shown in Fig. 5, this implies that  $\delta_1$  is above unity:  $\delta_1 \geq q \geq 1$ , whereas the minimal value of  $\delta_2$  is  $q^{-1} \leq 1$ . It is illustrated that the noise variances are positive provided the squeezing parameter  $r$  is ranged between the endpoints of the interval given by

$$r \in [r_2, r_1], \quad r_1 = \ln \delta_1^{1/2}, \quad r_2 = \ln \delta_2^{-1/2} \quad (73)$$

An important point is that the value of the squeezing parameter is generally not uniquely determined by the conditions (70). Referring to Fig. 5, the sole exception is provided by the limiting case of perfect homodyne measurements with  $\sigma_x^{(1)} = \sigma_x^{(2)} = 1$  and  $\delta_1 = \delta_2^{-1} = q$ . In this case, the squeezing parameter is uniquely defined by the imbalance ratio of the input beam splitter

$$r_1 = r_2 = \rho = \frac{1}{2} \ln q = \ln \sqrt{\frac{1 - C_S^2}{C_S^2}} \quad (74)$$

and the probability (49) expressed in terms of the distribution (67)

$$P_G^{(1)}(x_1, x_2) = \frac{\cosh \rho}{2\pi |\alpha_L^{(1)} \alpha_L^{(2)}|} |\langle ze^{i\phi}, \rho e^{2i\phi} | \alpha \rangle|^2, \quad (75)$$

yields the POVM

$$\begin{aligned} \hat{\Pi}_G^{(1)}(x_1, x_2) &= \frac{\cosh \rho}{2\pi |\alpha_L^{(1)} \alpha_L^{(2)}|} \\ &\times |\langle ze^{i\phi}, \rho e^{2i\phi} | \langle ze^{i\phi}, \rho e^{2i\phi} | \alpha \rangle|^2, \end{aligned} \quad (76)$$

which is proportional to the projector onto the pure squeezed state  $|ze^{i\phi}, \rho e^{2i\phi}\rangle$ . The result (74) was reported in Ref. [70].

When the homodyne measurements are not perfect due to unbalanced beam splitters and nonideal photodetectors, the squeezing parameter is no longer uniquely defined. So, in the interval (73), we have the decomposition of the probability (49)

$$\begin{aligned} P_G^{(\text{DH})}(x_1, x_2) &= \frac{\sqrt{\sigma_1 \sigma_2}}{2\pi \sqrt{\sigma_G^{(1)} \sigma_G^{(2)}}} \int d^2 \beta G(x_1 - \beta_1; \sigma_N^{(1)}(r)) \\ &\times G(x_2 - \beta_2; \sigma_N^{(2)}(r)) |\langle \beta e^{i\phi}, re^{2i\phi} | \alpha \rangle|^2, \end{aligned} \quad (77)$$

that varies with the squeezing parameter  $r$ . Similarly, the corresponding POVM

$$\begin{aligned} \hat{\Pi}_G^{(\text{DH})}(x_1, x_2) &= \frac{\sqrt{\sigma_1 \sigma_2}}{2\pi \sqrt{\sigma_G^{(1)} \sigma_G^{(2)}}} \int d^2 \beta G(x_1 - \beta_1; \sigma_N^{(1)}(r)) \\ &\times G(x_2 - \beta_2; \sigma_N^{(2)}(r)) |\beta e^{i\phi}, re^{2i\phi} \rangle \langle \beta e^{i\phi}, re^{2i\phi}|, \end{aligned} \quad (78)$$

decomposed into the Gaussian incoherent superposition of the pure squeezed states explicitly depends on the value of  $r$ .

Our analysis suggests that the ambiguity (non-uniqueness) of the Gaussian representation (78) for the double-homodyne POVM is a universal feature coming into play in the presence of imperfections. Even when  $\delta_2 \geq 1$  and the coherent-state representation (63) for the POVM is well-defined, the photocount statistics can be reproduced using the squeezed-state representation (78) with  $r \neq 0$ . Analogously, the density matrices of mixed Gaussian states can be expressed as randomly displaced squeezed states and, in general, this representation is non-unique. In the next section we demonstrate that the non-uniqueness of additive noise channel should be taken into account in certain scenarios of security analysis of continuous variable quantum key distribution protocols.

#### IV. MEASUREMENT IMPERFECTIONS AND SECURITY OF CONTINUOUS VARIABLE QUANTUM KEY DISTRIBUTION PROTOCOLS

In this section, we apply the developed formalism for asymmetric noisy Gaussian measurements to study how the measurement noise manifests itself in analysis of continuous variable quantum key distribution (CV-QKD) protocols (see, e.g., Ref. [43] for a recent review). Specifically, we concentrate on the Gaussian-modulated coherent-state (GMCS, or GG02) CV-QKD protocol suggested in [71] and examine how the measurement asymmetry affects its asymptotic security in the untrusted noise scenario [72].

##### A. Untrusted-noise scenario

In the GMCS protocol, the sender (Alice) prepares an ensemble of normally distributed coherent states  $|\alpha = \alpha_1 + i\alpha_2\rangle$  with the Gaussian probability density  $p_A(\alpha) = G(\alpha_1; V_A)G(\alpha_2; V_A)$ , so that the density matrix of the input state

$$\begin{aligned} \hat{\rho}_A &= \int d^2 \alpha p_A(\alpha) |\alpha\rangle \langle \alpha| = \Phi_A(|0\rangle \langle 0|), \\ p_A(\alpha) &= \frac{1}{\pi V_A} \exp \left[ -\frac{|\alpha|^2}{2V_A} \right] \end{aligned} \quad (79)$$

represents randomly displaced states generated by applying the additive noise channel  $\Phi_A$  with the covariance matrix  $\Sigma_A = 4V_A \mathbb{1}$  to the vacuum state  $|0\rangle \langle 0|$ . The states prepared by Alice are then transmitted to the receiver (Bob) through the quantum channel  $\mathcal{N}_{A \rightarrow B}$  which is assumed to be a composition of two Gaussian channels [72] given by

$$\mathcal{N}_{A \rightarrow B} = \Phi_\xi \circ \mathcal{E}_T, \quad (80)$$

where  $\mathcal{E}_T$  is the pure-loss channel with the transmittance  $T$  and  $\Phi_\xi$  is the additive noise channel with the noise covariance matrix  $\Sigma_\xi = \xi \mathbb{1}$ . In order to decode the signal, Bob measures the output state of the quantum channel (80).

This is a prepare-and-measure (PM) protocol, where the mutual information between Alice and Bob is determined by the joint probability distribution of the measurement outcomes and the components of the coherent state amplitude. It is not difficult to show (see Appendix C for technical details) that, when Bob performs homodyne detection, the mutual information is given by

$$I_{AB}^{(\text{H})} = \frac{1}{2} \log \left[ 1 + \frac{4TV_A}{\sigma_x + \xi} \right], \quad (81)$$

where  $\sigma_x$  is given by Eq. (17), whereas, if Bob uses double-homodyne detection, the expression for the mutual information takes the form

$$I_{AB}^{(\text{DH})} = \frac{1}{2} \sum_i \log \left[ 1 + \frac{4TV_A}{2\sigma_i + \xi} \right], \quad (82)$$

where  $\sigma_i$  are given by Eq. (53).

According to Eqs. (81) and (82), the mutual information depends on the type of measurement performed by Bob. This information enters the Devetak-Winter formula [73] for the asymptotic secret fraction (the number of secret bits that can be distilled per transmission of the signal)

$$K^{(\gamma)} = \beta I_{AB}^{(\gamma)} - \chi_{EB}^{(\gamma)}, \quad \gamma \in \{\text{H}, \text{DH}\}, \quad (83)$$

where  $0 < \beta < 1$  is the reconciliation efficiency and  $\chi_{EB}^{(\gamma)}$  is the Holevo information. This formula suggests

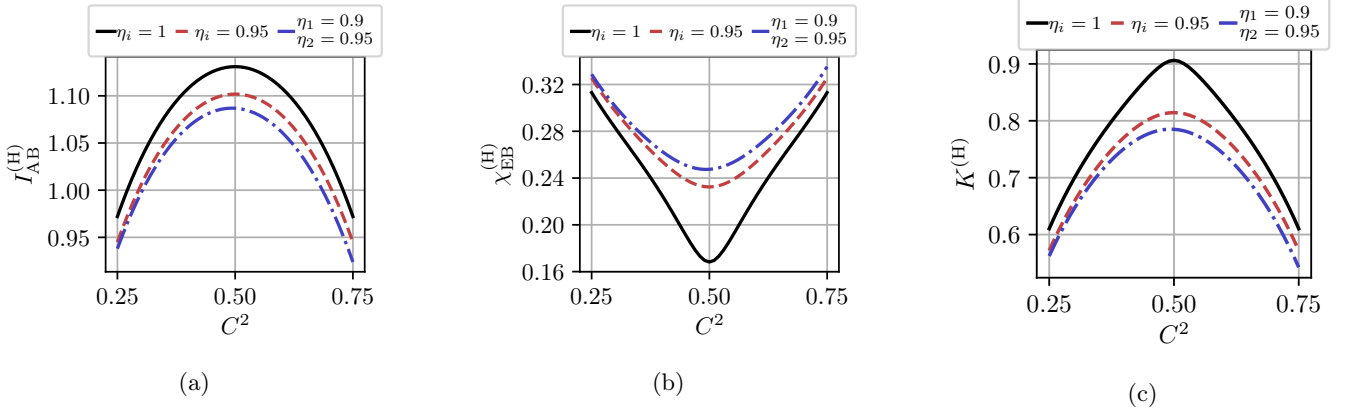


Figure 6: (a) Mutual information,  $I_{AB}^{(H)}$ , (b) Holevo information,  $\chi_{EB}^{(H)}$  and (c) asymptotic secret fraction,  $K^{(H)}$ , as a function of the beam splitter transmission,  $C^2$ , of the homodyne receiver (see Fig. 1) computed at different values of the detector efficiencies. The parameters are:  $V_A = 1$ ;  $T = 0.95$ ;  $\xi = 10^{-3}$ ; and  $\beta = 0.95$ .

using the entanglement-based (EB) version of the protocol, where Alice prepares a two-mode squeezed vacuum (TMSV) state, measures both quadratures of the first mode send the second mode to Bob. As discussed in Appendix C after Eq. (C9), the EB representation is equivalent to the PM protocol because both versions are indistinguishable from the perspective of the receiver and the eavesdropper (Eve).

In this picture, the covariance matrix of the bipartite quantum state shared by Alice and Bob,  $\hat{\rho}_{AB}$ , can be obtained from the TMSV covariance matrix with the Bob's mode transmitted through the noisy channel as follows (see Ref. [72])

$$\begin{aligned} \mathcal{I}_A \otimes \Phi_\xi \circ \mathcal{E}_T : \Sigma_{TMSV} \\ = \begin{pmatrix} V\mathbb{1} & \sqrt{V^2-1}\sigma_z \\ \sqrt{V^2-1}\sigma_z & V\mathbb{1} \end{pmatrix} \mapsto \Sigma_{AB} \\ = \begin{pmatrix} V\mathbb{1} & c\sigma_z \\ c\sigma_z & V_B\mathbb{1} \end{pmatrix}, \quad \sigma_z = \text{diag}(1, -1), \end{aligned} \quad (84)$$

where  $\mathcal{I}_A$  is the identity channel acting on the subsystem  $A$ ;  $\mathbb{1} = \text{diag}(1, 1)$  is the unity matrix; and the parameters of the covariance matrix  $\Sigma_{AB}$  are given by

$$V = 1 + 4V_A, \quad c = \sqrt{T(V^2 - 1)}, \quad (85)$$

$$V_B = T(V - 1) + 1 + \xi. \quad (86)$$

The standard approach to evaluation of the Holevo information is to assume that Eve holds a purification of  $\hat{\rho}_{AB}$  and use the property of extremality of Gaussian states [74, 75] to estimate the upper bound of the Holevo information from the covariance matrix  $\Sigma_{AB}$ .

In the untrusted-noise scenario, where additional noise responsible for detection imperfections is assumed to be accessible to Eve, the density matrix  $\hat{\rho}_{AB}$  should be modified. In our case, the noisy POVMs (see Eqs. (38) and (78)) are generated from the POVMs of ideal measurements by applying the dual of a Gaussian quantum

channel of the following form

$$\hat{\Pi}_G^{(\gamma)} = [\Phi_N^{(\gamma)}]^* (\hat{\Pi}_{id}^{(\gamma)}) = \Phi_N^{(\gamma)} (\hat{\Pi}_{id}^{(\gamma)}), \quad (87)$$

where  $\Phi_N^{(\gamma)}$  is the additive noise channel with the covariance matrix  $\Sigma_N^{(\gamma)}$  (Eqs. (34) and (69) give  $\Sigma_N^{(H)}$  and  $\Sigma_N^{(DH)}$ , respectively). When this channel is under control of the eavesdropper, Eve holds a purification of the state  $\hat{\rho}_{AB}^{(\gamma)} = \mathcal{I}_A \otimes \Phi_N^{(\gamma)}(\hat{\rho}_{AB})$  with the covariance matrix given by

$$\begin{aligned} \mathcal{I}_A \otimes \Phi_N^{(\gamma)} : \Sigma_{AB} \mapsto \Sigma_{AB}^{(\gamma)} \\ = \begin{pmatrix} V\mathbb{1} & c\sigma_z \\ c\sigma_z & V_B\mathbb{1} + \Sigma_N^{(\gamma)} \end{pmatrix}, \quad \gamma \in \{H, DH\} \end{aligned} \quad (88)$$

and the measurements performed by the receiver are assumed to be noiseless. This is the scenario of our primary concern. In this scenario, the difference between the joint and conditional entropies

$$\chi_{EB}^{(\gamma)} = S_E - S_{E|B} = S_{AB}^{(\gamma)} - S_{A|B}^{(\gamma)} \quad (89)$$

gives the Holevo information. The joint entropy

$$S_{AB}^{(\gamma)} = g(\nu_1^{(\gamma)}) + g(\nu_2^{(\gamma)}), \quad (90)$$

$$g(\nu) = \frac{\nu + 1}{2} \log \frac{\nu + 1}{2} - \frac{\nu - 1}{2} \log \frac{\nu - 1}{2} \quad (91)$$

then can be expressed in terms of the symplectic eigenvalues of the covariance matrix (88) given by

$$\nu_{1,2}^{(\gamma)} = \sqrt{\Delta_\gamma/2 \pm \sqrt{\Delta_\gamma^2/4 - D_\gamma}}, \quad D_\gamma = \det \Sigma_{AB}^{(\gamma)}, \quad (92)$$

$$\Delta_\gamma = \det(V_B\mathbb{1} + \Sigma_N^{(\gamma)}) + V^2 - 2c^2. \quad (93)$$

By applying the partial measurement formula [18] to the covariance matrix  $\Sigma_{AB}^{(\gamma)}$ , we also obtain the conditional covariance matrix

$$\Sigma_{A|B}^{(\gamma)} = V\mathbb{1} - c^2\sigma_z(V_B\mathbb{1} + \Sigma_m^{(\gamma)})^{-1}\sigma_z, \quad (94)$$

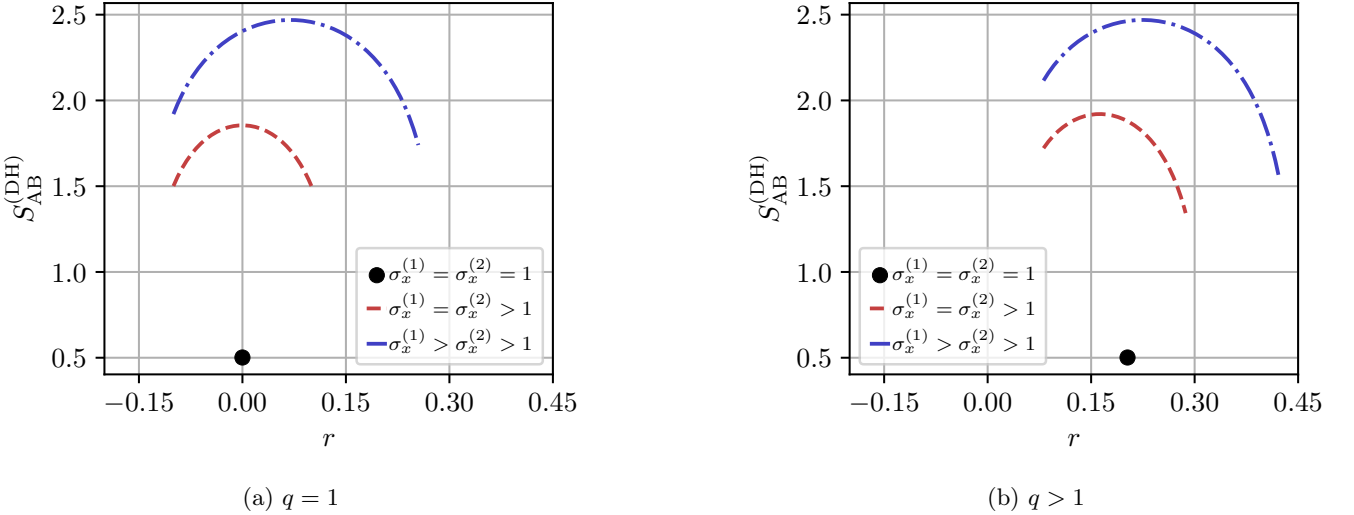


Figure 7: Joint entropy,  $S_{AB}^{(DH)}$ , as a function of the squeezing parameter  $r$  (see Eq. (73)) at different values of the quadrature variances  $\sigma_x^{(i)}$  (53) for (a) the balanced input beam splitter with the imbalance ratio (72),  $q$ , equal to unity and (b) the unbalanced input beam splitter. All other beam splitters are assumed to be balanced. The channel parameters are:  $V_A = 1$ ;  $T = 0.95$ ; and  $\xi = 10^{-3}$ .

so that the conditional entropy  $S_{E|B} = S_{A|B}^{(\gamma)}$  reads

$$S_{A|B}^{(\gamma)} = g(\nu_3^{(\gamma)}), \quad \nu_3^{(\gamma)} = \sqrt{\det \Sigma_{A|B}^{(\gamma)}}, \quad (95)$$

where  $\nu_3^{(\gamma)}$  is the simplectic eigenvalue of  $\Sigma_{A|B}^{(\gamma)}$ . For homodyne detection, we have

$$\nu_3^{(H)} = \sqrt{V \left( V - \frac{c^2}{V_B + \sigma_N} \right)}, \quad (96)$$

whereas, for double homodyne detection, the result is

$$\nu_3^{(DH)} = V \sqrt{\frac{(V_B + \delta_1 - \frac{c^2}{V})(V_B + \delta_2 - \frac{c^2}{V})}{(V_B + \delta_1)(V_B + \delta_2)}}, \quad (97)$$

where  $\delta_i = 2\sigma_i - 1$  is given by Eq. (71).

## B. Numerical results

Our analytical results for the mutual information (see Eqs. (81) and (81)) and the entropies (see Eqs. (90) and (94)) that enter the expression for the Holevo information (89) can now be used to quantify the asymmetry and imbalance induced effects of noisy measurements. One of the key points is that, in the untrusted-noise scenario, the Holevo information explicitly depends on the dual channel representation of noisy POVMs given by Eq. (87).

In the case of homodyne detection, the ideal measurements are described by the quadrature eigenstate projectors and the additive noise channel representation is

uniquely determined by the excess noise covariance matrix (34). Figure 6 shows how the mutual information, the Holevo information and the secret key fraction depend on the transmittance of the beam splitter used in the homodyne detection scheme (see Fig. 1). It is seen that, in general, the beam splitter imbalance has a detrimental effect on performance of the protocol. Interestingly, in the presence of asymmetry in efficiencies of the photodetectors, both the mutual information and secret fraction can be maximized by introducing a suitably unbalanced beam splitter. Similar remark applies to minimization of the Holevo information. Qualitatively, behavior of the curves presented in Fig. 6 are in agreement with the corresponding results reported in Ref. [76] such as dependence of the asymptotic secret fraction on the beam splitter transmittance deviation and balanced detector deviation.

By contrast to homodyne detection, the channel representation for the POVM of noisy double homodyne measurements (78) appears to be dependent on the properties of the pure squeezed states (65) describing the noiseless POVMs. According to Eq. (69), the squeezing parameter,  $r$ , that lies in the interval (73) explicitly enters the expression for the excess noise covariance matrix,  $\Sigma_N^{(DH)}$ . The latter makes the covariance matrix (88),  $\Sigma_{AB}^{(DH)}$ , and the joint (Eve's) entropy (90),  $S_{AB}^{(DH)}$ ,  $r$ -dependent. Hence it turned out that the Holevo information is a function of  $r$ .

Figure 7 illustrates dependence of the joint (Eve's) entropy,  $S_{AB}^{(DH)}$ , on the squeezing parameter. Referring to Fig. 7, in the limiting case of ideal double homodyne with  $\sigma_x^{(1)} = \sigma_x^{(2)} = 1$ , the only allowed value of  $r$ ,  $r = \rho$ , is

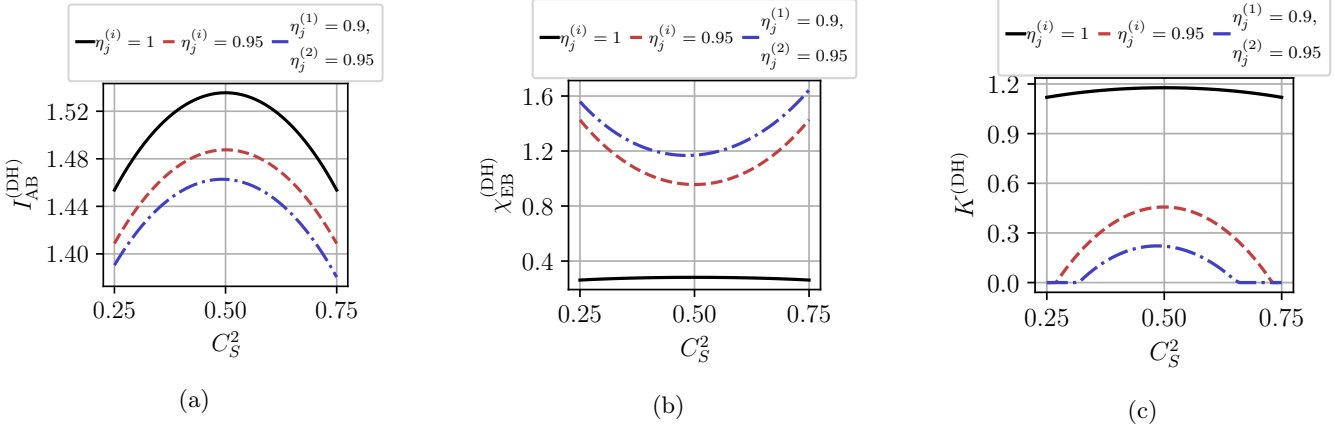


Figure 8: (a) Mutual information,  $I_{AB}^{(DH)}$ , (b) Holevo information,  $\chi_{EB}^{(DH)}$  and (c) asymptotic secret fraction,  $K^{(DH)}$ , as a function of the signal beam splitter transmission,  $C_S^2$ , of the double homodyne receiver (see Fig. 3) computed at different values of the detector efficiencies. All other beam splitters are assumed to be balanced and efficiencies not specified in the legend are taken to be unity. The parameters are:  $V_A = 1$ ;  $T = 0.95$ ;  $\xi = 10^{-3}$ ; and  $\beta = 0.95$ .

given by Eq. (74) and the corresponding value of entropy is marked by the black dot. Otherwise, the endpoints of the interval (73) differ.

When the input (signal) beam splitter is balanced and the imbalance ratio (72) equals unity,  $q = 1$ , all the curves shown in Fig. 7a contain the zero-squeezing point with  $r = 0$  representing the coherent-state limiting case (63). It can be seen that the maximum of the entropy is located at this point provided the homodyne detection variances are identical with  $\sigma_x^{(1)} = \sigma_x^{(2)}$ . This is, however, no longer the case when the symmetry is broken and  $\sigma_x^{(1)} \neq \sigma_x^{(2)}$ .

Since, in the scenario under consideration, Eve controls the measurement noise channel, the freedom to choose the value of  $r$  can be used to maximize the information available to the eavesdropper. This strategy is equivalent to maximizing the entropy  $S_{AB}^{(DH)}$  that leads to the coherent-state representation of double homodyne POVM only if  $q = 1$  and  $\sigma_x^{(1)} = \sigma_x^{(2)}$ .

In other cases, the optimal value of  $r$  differs from zero and corresponds to the squeezed-state representation (78). The curves depicted in Fig. 7b demonstrate that, at  $q \neq 1$ , the zero-squeezing point can be outside the squeezing parameter interval (73). This is the case when the entropy  $S_{AB}^{(DH)}$  is ill-defined at  $r = 0$  due to the presence of symplectic eigenvalues that are smaller than unity.

For calculations, we will optimize  $r$  to maximize  $\chi_{EB}$ .

The graphs presented in Fig. 8, similar to Fig. 7, show the mutual information, the Holevo information and the secret key fraction computed as a function of the input (signal) beam splitter transmittance of the double homodyne scheme (see Fig. 3). In these calculations, the value of the squeezing parameter is taken to be optimal so that the Holevo information is maximized at  $r = r_{\text{opt}} = \arg \max_r \chi_{EB}^{(DH)}(r)$ .

Qualitatively, the curves plotted in Fig. 8 reveal behavior similar to the ones evaluated for homodyne detection (see Fig. 6). A comparison between Fig. 6a and Fig. 8a shows that, as is expected, the mutual information for double homodyne detection generally exceeds the information for homodyne detection,  $I_{AB}^{(DH)} > I_{AB}^{(H)}$ . For noiseless detection with  $\sigma_x^{(1)} = \sigma_x^{(2)} = 1$  (black solid curves in Figs. 8 and 6), the resulting double-homodyne asymptotic secret fraction plotted in Fig. 8c is noticeably higher than the value computed for the homodyne detection shown in Fig. 6c,  $K^{(DH)} > K^{(H)}$ . In this case, an interesting feature illustrated by the black curve for the Holevo information (see Fig. 8b) is that imbalance of the input (signal) beam splitter results in decreased Holevo information. The reason is that, in the limit of ideal detection, the excess noise variances,  $\sigma_N^{(1)}$  and  $\sigma_N^{(2)}$ , are both equal to zero and the entropy  $S_{AB}^{(DH)}$  is independent of  $C_S^2$ , whereas the conditional entropy  $S_{A|B}^{(DH)}$ , being an even function of  $1/2 - C_S^2$ , grows with imbalance.

When the measurements are noisy, the dashed and dash-dotted curves plotted in Figs. 6b and 8b indicate a noise induced increase of the Holevo information so that its value for double homodyne detection appears to be significantly larger than the homodyne Holevo information. As a consequence it turned out that the double-homodyne secret fraction  $K^{(DH)}$  is lower than  $K^{(H)}$  (see Figs. 6c and 8c).

This effect can also be observed in Fig. 9 that presents dependencies of the asymptotic secret fraction on the channel length evaluated for both the homodyne and double homodyne detection (see Figs. 9a and 9b, respectively). From Fig. 9, it is clear that, in the untrusted-noise scenario, imperfections of measurements have a detrimental effect on the performance of the protocol significantly reducing the maximal channel length (the

transmission distance). It is also seen that, for double homodyne measurements, deterioration in performance is more pronounced as compared to the case of homodyne detection. Note that the dash-dotted curves in Fig. 9 illustrate effects of asymmetry in photodetector efficiencies that results in degraded performance. The latter is in a qualitative agreement with the results recently reported in Ref. [62] for different scenario.

## V. DISCUSSION AND CONCLUSION

In this paper, we have studied the effects of asymmetry introduced by unbalanced beam splitters and different efficiencies of the photodetectors in photocount statistics of homodyne and double homodyne detection. By using the Gaussian approximation derived by approximating the Poisson distributions with the probability density functions of normally distributed random variables, we have computed the  $Q$  symbols of the POVMs of noisy homodyne and double homodyne (heterodyne) measurements. (Applicability range of the Gaussian approximation is discussed in Appendix A.) Similar to Gaussian states, these POVMs are generally characterized by the mean quadratures and the covariance matrix.

For homodyne measurements, we have used the  $Q$  symbol (15) to deduce the homodyne covariance matrix (33). The operator representation of the noisy homodyne POVM (38) is derived by applying the additive noise (classical mixing) channel (22) with the excess noise covariance matrix (34) to the POVM of the noiseless (ideal) measurements (27) described by the projectors onto the quadrature eigenstates (28). Such representation arises as a natural result of our general approach which is outlined in Sec. II B and is based on the well-known fact that a POVM of a noisy Gaussian measurement can be obtained as a POVM of a projective Gaussian measurement transformed under the action of the dual of a suitably chosen Gaussian channel [18].

When this approach is applied to the case of double homodyne measurements (the asymmetric eight-port double homodyne scheme is illustrated in Fig. 3) with the  $Q$  symbol (49) and the covariance matrix (54), we have shown that the class of noiseless measurements should be extended so as to include the squeezed-state projective measurements (these states are given by Eq. (65)) with the squeezing parameter ranged between the endpoints of the interval (73). It was found that the squeezed-state operator representation of the double-homodyne POVM (78) emerges from such the POVMs of the noiseless squeezed-state measurements under the action of the additive noise channel with the excess noise covariance matrix (69). So, the asymmetry induced anisotropy of the distributions in the photocount difference plane illustrated in Fig. 4 leads to the ambiguity of the operator representation of the double-homodyne POVM that appears to be dependent on the squeezing parameter.

We have demonstrated that this inherent non-

uniqueness of the POVM representation becomes relevant when analyzing the asymptotic security of the Gaussian-modulated CV-QKD protocol in the untrusted-noise scenario. Specifically, we have studied how asymmetry of the noisy measurements impacts the performance of CV-QKD system in the scenario where the measurement noise is accessible to Eve.

In this scenario, the upper bound for the Holevo information is estimated by assuming that the covariance matrix of the state shared by Alice and Bob is additionally transmitted through the channel describing the noise of Bob's measurements. Since this state is purified by Eve, the Eve's (joint) entropy explicitly depends on the parameters of the measurement noise channel. In our case, this channel is chosen to be the additive noise channel (22) with the excess noise covariance matrix given by Eqs. (34) and (69) for homodyne and double homodyne measurements, respectively. It was found that, for both types of the measurements, the mutual information, the Holevo information and the asymptotic secret fraction are sensitive to asymmetry effects (see Figs. 6 and 8). These effects result in degraded performance of the protocol leading to a significant reduction in the maximum channel length (see Fig. 9).

A distinguishing feature of the double homodyne detection is that we have to deal with the squeezing dependent joint (Eve's) entropy (see Fig. 7). Since Eve controls the channel, the latter has to be optimized. In other words, for the curves presented in Fig. 8, the optimal values of the squeezing parameter are found by performing maximization of the Holevo information.

In this study, for illustrative purposes, we have restricted our attention to the case of the untrusted-noise scenario. The opposite case of the trusted-noise (device) scenario [77–79] is beyond the scope of this paper as it requires an additional and a more sophisticated analysis which is the subject of a separate publication.

In conclusion, we put our results in the general context of CV-QKD security [43]. The asymmetry effects described in the paper, such as deviations from the ideal 50:50 beam splitter ratio and mismatched detector efficiencies, introduce vulnerabilities into CV-QKD systems. These flaws not only allow quantum hackers to compromise security but also degrade the system's performance [61]. These vulnerabilities can be exploited by adversaries through attack strategies such as the wavelength attack [53, 54] and the homodyne detector blinding [55] and saturation [56]. The wavelength attack leverages the wavelength-dependent coupling ratio of fiber beam splitters and can be countered by using proper spectral filtering. Blinding and saturation attacks exploit the saturation behavior of homodyne detectors, and their effectiveness is amplified by receiver imbalance. If the splitting ratio deviates from ideal one, an injected bright pulse more easily displaces the detector output, facilitating saturation and biasing excess noise estimation.

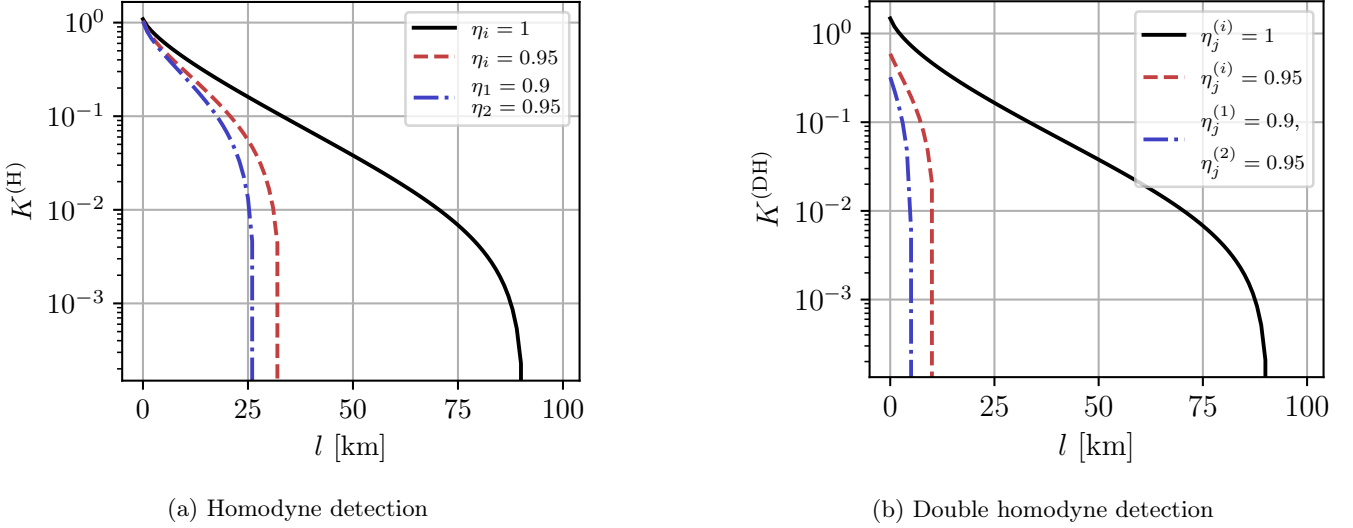


Figure 9: Asymptotic secret fraction as a function of channel length computed for (a) homodyne detection and (b) double homodyne detection at various detector efficiencies. The losses are assumed to be 20 dB per 100 km. The parameters are:  $V_A = 1$ ;  $\xi = 10^{-3}$ ; and  $\beta = 0.95$ .

## ACKNOWLEDGMENTS

The work was supported by the Russian Science Foundation (project No. 24-11-00398).

## Appendix A: Statistical distance between Gaussian approximation and Skellam distribution

In this Appendix, we study the performance of Gaussian approximation for the statistics of photon count difference (10):

$$P_G(\mu) = G(\mu - \mu_G; \sigma_G), \quad (A1)$$

$$\sigma_G = \eta_1 |\alpha_1|^2 + \eta_2 |\alpha_2|^2 \approx (\eta_1 S^2 + \eta_2 C^2) |\alpha_L|^2, \quad (A2)$$

$$\begin{aligned} \mu_G &= \eta_1 |\alpha_1|^2 - \eta_2 |\alpha_2|^2 \approx (\eta_1 S^2 - \eta_2 C^2) |\alpha_L|^2 \\ &+ CS(\eta_1 + \eta_2) |\alpha_L| \langle \hat{x}_\phi \rangle \end{aligned} \quad (A3)$$

by comparing it with the exact statistics of difference events governed by the Skellam distribution (7):

$$\begin{aligned} P(\mu) &= e^{-\eta_1 |\alpha_1|^2} e^{-\eta_2 |\alpha_2|^2} \left( \frac{\eta_1 |\alpha_1|^2}{\eta_2 |\alpha_2|^2} \right)^{\mu/2} \\ &\times I_\mu(2\sqrt{\eta_1 \eta_2 |\alpha_1|^2 |\alpha_2|^2}), \end{aligned} \quad (A4)$$

both repeated here for ease. We limit our numerical results to the coherent signal state only, except in cases where the curves show sufficiently distinct differences.

We evaluate the statistical distance between the probability distributions using the total variational distance that can be computed as half of the  $L^1$  distance

$$D_P \equiv D(P, P_G) \equiv \frac{1}{2} \sum_{\mu=-\infty}^{\infty} |P(\mu) - P_G(\mu)|. \quad (A5)$$

Note that, according to Eq. (A5),  $\mu$  takes integer values and we evaluate the distance between the probability mass fractions, whereas the normalization condition for the Gaussian function (A1)

$$\int_{-\infty}^{\infty} d\mu P_G(\mu) = 1 \quad (A6)$$

implies applicability of the continuum limit. For integer  $\mu$ , the integral on the left hand side of Eq. (A6) should be replaced with a sum and we have the relation

$$\sum_{\mu=-\infty}^{\infty} P_G(\mu) = \vartheta_3(\pi \mu_G, e^{-2\pi^2 \sigma_G}) \equiv N_G \quad (A7)$$

where  $\vartheta_3$  is the Jacobi elliptic theta function [65].

In the applicability region of the continuum limit, the normalization constant  $N_G$  is close to unity. The numerical analysis shows that  $|N_G - 1| \leq 10^{-4}$  at  $2\sigma_G \geq 1$ . The latter gives the condition for the LO amplitude

$$|\alpha_L| \geq \frac{1}{\sqrt{2(\eta_1 S^2 + \eta_2 C^2)}} \equiv \alpha_N \quad (A8)$$

which ensures both applicability of the continuum limit and proper normalization of the Gaussian approximation. In our calculations, the probability  $P_G$  will be numerically corrected by introducing the factor  $N_G^{-1}$  provided that  $|\alpha_L|$  is below the "renormalization point"  $\alpha_N$ .

The curves presented in Fig. 10 illustrate how the accuracy of the Gaussian approximation is affected by the signal and LO amplitudes,  $|\alpha|$  and  $|\alpha_L|$ . More specifically, in Fig. 10a (Fig. 10b), the statistical distance is numerically evaluated as a function of the amplitude  $|\alpha|$

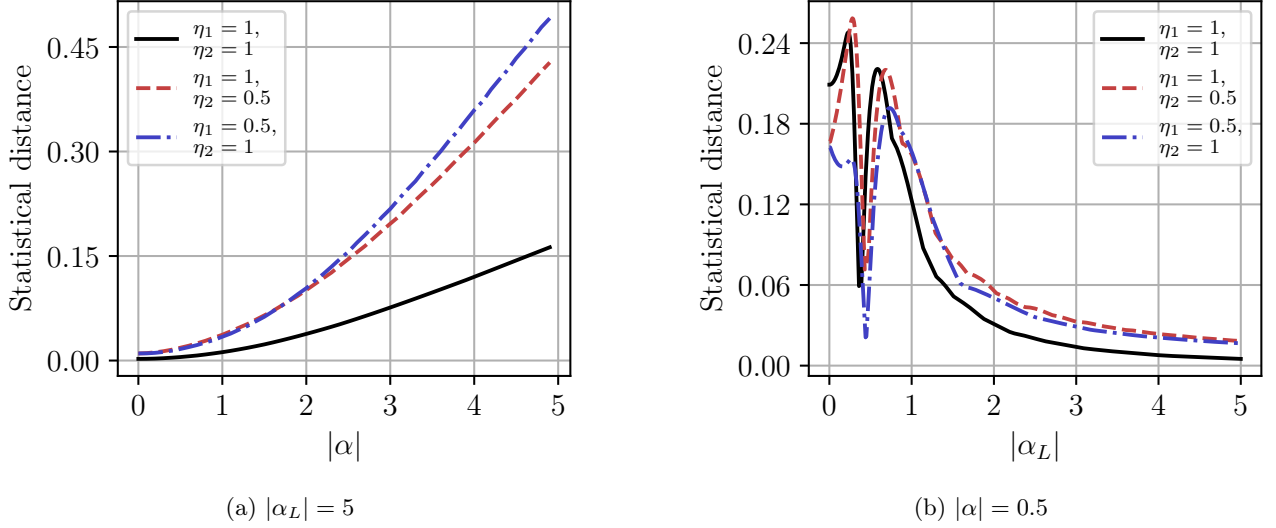


Figure 10: Statistical distance  $D_P = D(\mathcal{P}, \mathcal{P}_G)$  as a function of (a) signal amplitude and (b) LO amplitude at different detector efficiencies.

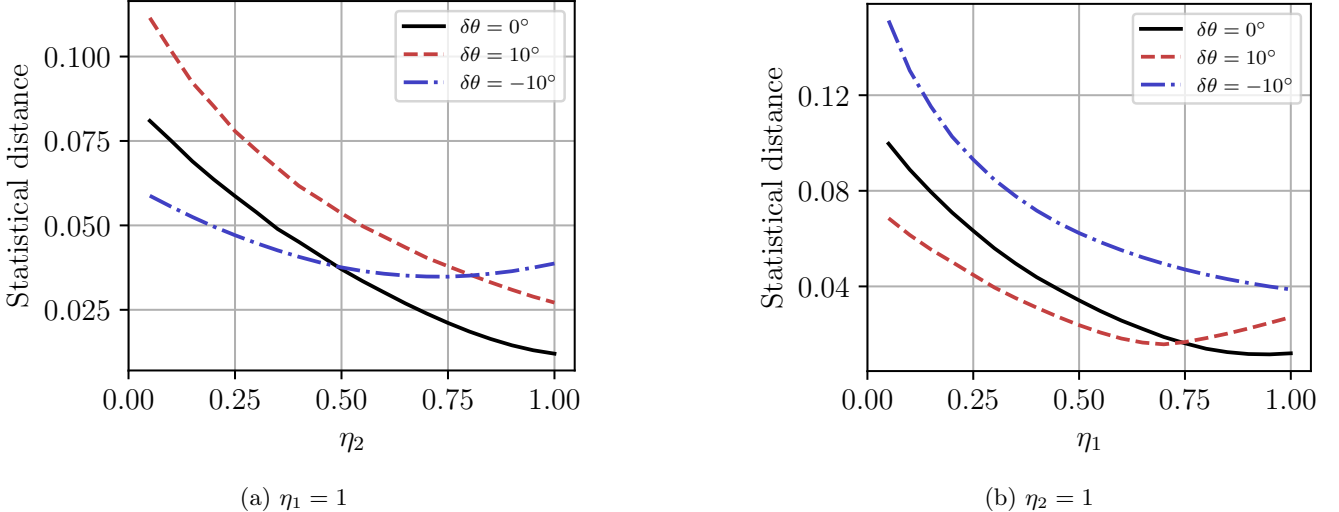


Figure 11: Statistical distance  $D_P = D(\mathcal{P}, \mathcal{P}_G)$  as a function of photodetector efficiency (a)  $\eta_2$  at  $\eta_1 = 1$  and (b)  $\eta_1$  at  $\eta_2 = 1$  for different values of the beam splitter imbalance angle  $\delta\theta$  (see eq. (A9)). The amplitudes are  $|\alpha| = 1$  and  $|\alpha_L| = 5$ .

( $|\alpha_L|$ ) at different values of the photodetectors efficiencies provided that the value of the other amplitude  $|\alpha_L|$  ( $|\alpha|$ ) is fixed.

Referring to Fig. 10a, the curves behave as expected: given the LO amplitude  $|\alpha_L|$ , the distance monotonically increases with  $|\alpha|$ . It is shown that, at  $|\alpha_L| = 5$  and  $|\alpha| > 1$ , the perfectly symmetric homodyne presents the case with minimal distance,  $D_P$ , while in the presence of asymmetry, the curves exhibit a rapid growth and the quality of the Gaussian approximation rapidly degrades to the point, where  $D_P > 0.1$ , so it is not useful for its intended purpose.

When it comes to dependencies of the statistical dis-

tance on the LO oscillator amplitude computed at fixed value of  $|\alpha|$ , the above results suggest that the smaller the amplitude  $|\alpha|$  the better the accuracy of the Gaussian approximation. We can also expect the distance will be small provided that  $|\alpha_L|$  is large and the strong-LO approximation is applicable.

Referring to Fig. 10b, the curves evaluated at  $|\alpha| = 0.5$  display a non-monotonic behavior with two local maxima in the weak LO range where  $|\alpha_L| < 1$ . By contrast, after the second maximum at  $|\alpha_L| > 1$ , the distance falls with the LO amplitude and it drops below 0.05 at  $|\alpha_L| > 2$ .

Note, that, when  $|\alpha| < 0.1$  and the signal mode state is close to the vacuum state, the two local maxima

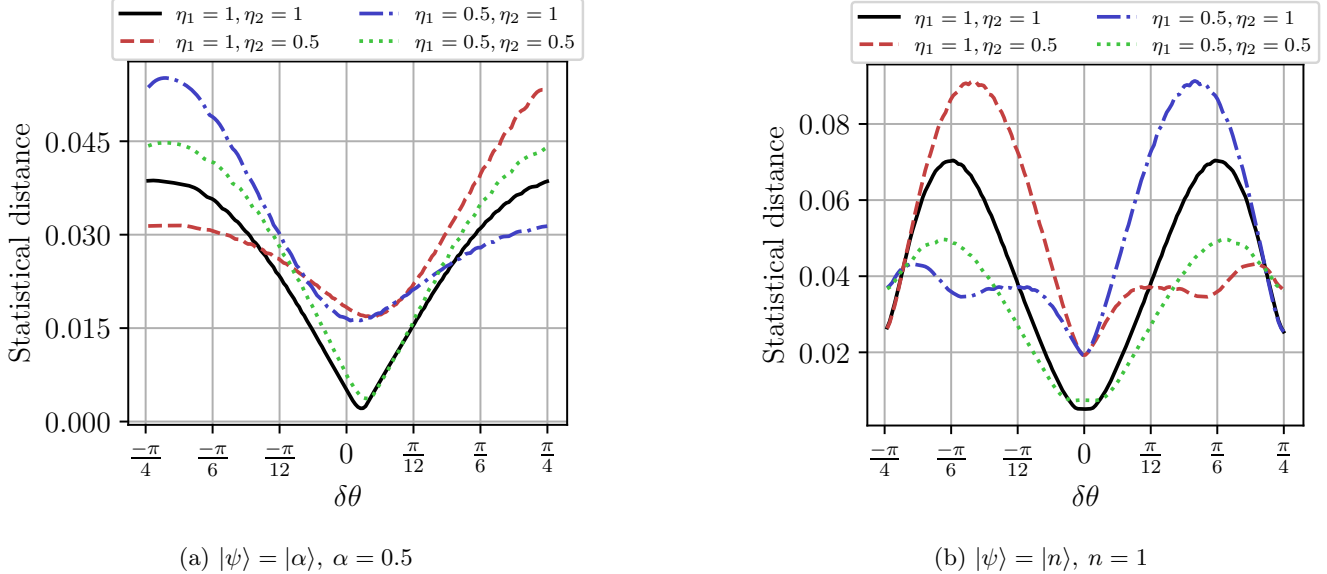


Figure 12: Statistical distance  $D_P = D(\mathcal{P}, \mathcal{P}_G)$  as a function of the beam splitter imbalance angle,  $\delta\theta$ , for the signal mode prepared in (a) the coherent state and in (b) the single photon Fock state at different efficiencies with  $|\alpha_L| = 5$ .

of  $D_P$  can be estimated to be slightly above 0.08 and 0.1, respectively. So, in this case, the distribution (10) might be regarded as a reasonable approximation even in the weak LO range where the probability  $\mathcal{P}_G$  approaches the close neighborhood of the singular limit,  $\lim_{|\alpha_L| \rightarrow 0} \mathcal{P}_G(\mu) = \delta(\mu)$ .

From Fig. 10b, it can also be seen that the distance vs LO amplitude dependence that can be used as a tool to characterize the applicability region of the strong-LO approximation is nearly insensitive to asymmetry. In other words, the latter does not produce noticeable effects on the accuracy of the approximation.

The parameters describing the photodetection asymmetry are the efficiencies  $\eta_1$  and  $\eta_2$ . The curves plotted in Fig. 10 are computed at different values of the efficiencies.

To quantify deviation of the beam splitter transmission and reflection amplitudes from the balanced 50 : 50 values  $t = \cos \theta = r = \sin \theta = 1/\sqrt{2}$  at the angle  $\theta = \pi/4$ , we introduce the beam splitter *imbalance angle* given by

$$\delta\theta \equiv \frac{\pi}{4} - \theta. \quad (\text{A9})$$

In Figure 11 we plot the distance against the efficiency of the photodetector assuming that the other photodetector is perfect. The curves are evaluated at different values of the imbalance angle (A9).

In Fig. 12 the statistical distance vs imbalance angle curves are presented for coherent and one-photon signal states. These curves illustrate how the beam splitter imbalance and the photodetector efficiencies influence the accuracy of the Gaussian approximation. The distance is shown to be minimal in the vicinity of the balanced beam splitter point with a vanishing imbalance angle,

$\delta\theta = 0$ . The efficiency dependence of the distance is shown to decrease monotonically at  $\delta\theta = 0$ . In contrast, for unbalanced beam splitter, this dependence can reveal non-monotonic behavior.

## Appendix B: Gaussian approximation from Skellam distribution

The derivation procedure for the Gaussian approximation outlined in Sec. II transforms the photocount difference probability (6) into the form of a convolution of the normal distributions by approximating the Poisson distributions. In this Appendix, we discuss an alternative method where the starting point is the Skellam distribution (7). For convenience, we shall reproduce the expression for this distribution here:

$$P(\mu) = e^{-\eta_1|\alpha_1|^2} e^{-\eta_2|\alpha_2|^2} \left( \frac{\eta_1|\alpha_1|^2}{\eta_2|\alpha_2|^2} \right)^{\frac{\mu}{2}} \times I_\mu \left( 2\sqrt{\eta_1\eta_2|\alpha_1|^2|\alpha_2|^2} \right), \quad (\text{B1})$$

where  $I_k(z)$  is the modified Bessel function of the first kind and the amplitudes  $|\alpha_{1,2}|$  are given by Eq. (3).

The method under consideration (see, e.g. the textbook [1]) assumes that, in the strong LO limit, the argument of the modified Bessel function is large and  $I_\mu(z)$  can be approximated using its asymptotic expansion taken in the Gaussian form:

$$I_\mu(z) \approx \frac{1}{\sqrt{2\pi z}} \exp \left[ z - \frac{\mu^2}{2z} \right]. \quad (\text{B2})$$

This formula can be deduced by performing a saddle-point analysis for the integral representation of the Bessel functions [80].

Heuristically, it can also be obtained from the lowest order asymptotic expansion for the Bessel function [65]:  $I_\mu(z) \approx e^z (1 - (4\mu^2 - 1)/(8z))/\sqrt{2\pi z}$  assuming that, for small values of  $x$ ,  $1 - x$  can be replaced with  $e^{-x}$  (the factors independent of  $\mu$  are not essential because they can be incorporated into the normalization factor of the Gaussian approximation).

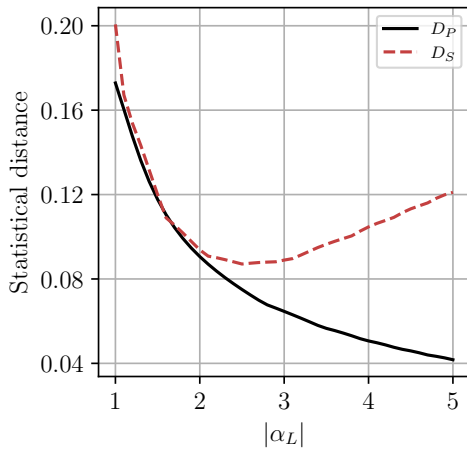


Figure 13: Distances,  $D_P = D(\mathbb{P}, \mathbb{P}_G)$  and  $D_S = D(\mathbb{P}, \mathbb{P}_G^{(s)})$ , between the Skellam distribution,  $\mathbb{P}$ , and two Gaussian approximations,  $\mathbb{P}_G$  (see Eq. (10)) and  $\mathbb{P}_G^{(s)}$  (see Eq. (B5)), as a function of  $|\alpha_L|$  the beam splitter imbalance angle at  $\delta\theta = 15^\circ$   $\alpha = 1$ , and  $\eta_1 = \eta_2 = 1$ .

Assuming that  $CS \neq 0$  and  $|\alpha_L|$  is sufficiently large, we can use the approximate relations

$$z = 2\sqrt{\eta_1\eta_2}|\alpha_1||\alpha_2| \approx 2CS\sqrt{\eta_1\eta_2}|\alpha_L|^2, \quad (B3)$$

$$\ln\left(\frac{\eta_1|\alpha_1|^2}{\eta_2|\alpha_2|^2}\right)^{\frac{C}{2}} \approx \frac{\mu}{2} \left( \ln\frac{\eta_1S^2}{\eta_2C^2} + \frac{\langle\hat{x}_\phi\rangle}{CS|\alpha_L|} \right) \quad (B4)$$

to obtain the Gaussian approximation for the Skellam distribution (B1) given by

$$\mathbb{P}_G^{(s)}(\mu) = G(\mu - \tilde{\mu}_G; \tilde{\sigma}_G), \quad (B5)$$

$$\tilde{\mu}_G = \sqrt{\eta_1\eta_2} \left[ CS|\alpha_L|^2 \ln \frac{\eta_1S^2}{\eta_2C^2} + |\alpha_L|\langle\hat{x}_\phi\rangle \right], \quad (B6)$$

$$\tilde{\sigma}_G = 2CS\sqrt{\eta_1\eta_2}|\alpha_L|^2. \quad (B7)$$

Similar to Eq. (15), we cast the probability (B5) into

the following quadrature form:

$$\mathbb{P}_G^{(s)}(\tilde{x}) = \frac{1}{\sqrt{2\pi\tilde{\sigma}_G}} \exp\left\{-\frac{(\tilde{x} - \langle\hat{x}_\phi\rangle)^2}{2\tilde{\sigma}_x^2}\right\}, \quad (B8)$$

$$\tilde{x} = \frac{\mu}{\sqrt{\eta_1\eta_2}|\alpha_L|} - CS|\alpha_L| \ln \frac{\eta_1S^2}{\eta_2C^2}, \quad (B9)$$

$$\tilde{\sigma}_x = \frac{2CS}{\sqrt{\eta_1\eta_2}}, \quad (B10)$$

so that we may follow the line of reasoning presented in Sec. II to deduce the POVM

$$\hat{\Pi}_G^{(s)} = \frac{1}{\sqrt{\eta_1\eta_2}|\alpha_L|} \times \int dx' G(x - x'; \tilde{\sigma}_N) |x', \phi\rangle\langle x', \phi| \quad (B11)$$

with the noise variance

$$\tilde{\sigma}_N = \tilde{\sigma}_x - 1, \quad 0 \leq \tilde{\sigma}_x \leq \tilde{\sigma}_x^{(\max)} = 1/\sqrt{\eta_1\eta_2}. \quad (B12)$$

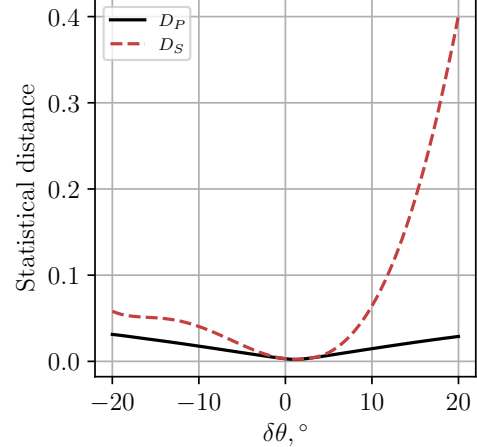


Figure 14: Distances,  $D_P = D(\mathbb{P}, \mathbb{P}_G)$  and  $D_S = D(\mathbb{P}, \mathbb{P}_G^{(s)})$ , between the Skellam distribution,  $\mathbb{P}$ , and two Gaussian approximations,  $\mathbb{P}_G$  (see Eq. (10)) and  $\mathbb{P}_G^{(s)}$  (see Eq. (B5)), as a function of the beam splitter imbalance angle  $\delta\theta$  at  $\alpha = 1$ ,  $\alpha_L = 10$  and  $\eta_1 = \eta_2 = 1$ .

Note that, in the symmetric case with  $C = S$  and  $\eta_1 = \eta_2$ , the Gaussian distributions given by Eqs. (10) and (B5) are equivalent. This is no longer the case in the presence of asymmetry effects.

Figure 13 demonstrates that, at  $\delta\theta \neq 0$ , by contrast to the distance between  $P$  and  $\mathbb{P}_G$ ,  $D_P = D(\mathbb{P}, \mathbb{P}_G)$  which is a monotonically decreasing function of  $|\alpha_L|$ , the distance between the Skellam distribution and the approximate distribution (B5),  $D_S = D(\mathbb{P}, \mathbb{P}_G^{(s)})$ , reveals non-monotonic behavior and increases with  $|\alpha_L|$  at sufficiently large LO amplitudes. Referring to Fig. 14, imbalance of the beam splitter has strong detrimental effect on the accuracy of the approximation (B5).

What is more important is that, by contrast the noise excess variance (35) which is always positive, the variance (B12) becomes negative when  $2CS \leq \sqrt{\eta_1\eta_2}$ . The latter breaks applicability of Eq. (B11) giving an ill-posed POVM.

### Appendix C: Mutual information and input state of entanglement-based representation

In this appendix, we begin with derivation of the expressions for the mutual information between Alice and Bob in the Gaussian-modulated coherent-state CV-QKD protocol discussed in Sec. IV. These expressions are given by Eqs. (81) and (82).

The important point greatly simplifying calculations is that both the channel (80) and the measurements are Gaussian. As a result, the random variables that determine the mutual information appear to be normally distributed, so that we can use the well-known analytical result that expresses the mutual information of the Gaussian random variables in terms of the determinants of the suitably defined covariance matrices (see, e.g., calculations detailed in online book [81]).

Specifically, transformations that a coherent state undergoes under the action of the channel  $\mathcal{N}_{A \rightarrow B}$  can be explicitly represented as follows

$$|\alpha\rangle\langle\alpha| \xrightarrow{\mathcal{E}_T} |\sqrt{T}\alpha\rangle\langle\sqrt{T}\alpha| \xrightarrow{\Phi_\xi} N_\xi \int d^2\beta \exp\left\{-\frac{2|\beta|^2}{\xi}\right\} \times |\sqrt{T}\alpha + \beta\rangle\langle\sqrt{T}\alpha + \beta|, \quad (C1)$$

where  $N_\xi = 2/(\pi\xi)$ . When Bob performs a Gaussian measurement described by the POVM  $\{\hat{\Pi}_G^{(\gamma)}(x)\}_x$ , where the value of  $x$  labels the measurement outcomes (e.g., for homodyne detection,  $x$  is the quadrature variable given by Eq. (16)), the joint probability density can be computed as follows

$$p_B^{(\gamma)}(x, \alpha) = p_B^{(\gamma)}(x|\alpha)p_A(\alpha), \quad \gamma \in \{H, DH\} \quad (C2a)$$

$$\begin{aligned} p_B^{(\gamma)}(x|\alpha) &= \text{Tr}\{\mathcal{E}_{A \rightarrow B}(|\alpha\rangle\langle\alpha|)\hat{\Pi}_G^{(\gamma)}(x)\} \\ &= \text{Tr}\{\mathcal{E}_T(|\alpha\rangle\langle\alpha|)\Phi_\xi^*(\hat{\Pi}_G^{(\gamma)}(x))\} \\ &= \langle\sqrt{T}\alpha|\Phi_\xi(\hat{\Pi}_G^{(\gamma)}(x))|\sqrt{T}\alpha\rangle, \end{aligned} \quad (C2b)$$

where we have used the fact that the additive noise channel  $\hat{\Phi}_\xi$  is self-dual:  $\hat{\Phi}_\xi^* = \hat{\Phi}_\xi$ .

For homodyne detection, we can combine Eq. (C2) and the expression for the  $Q$  symbol of POVM given by Eq. (15) to deduce the joint probability density

$$\begin{aligned} p_B^{(H)}(x, \tilde{\alpha}_1) &\propto \exp\left[-\frac{(x - 2\tilde{\alpha}_1)^2}{2(\sigma_x + \xi)} - \frac{\tilde{\alpha}_1^2}{2TV_A}\right] \\ &= \exp\left\{-\frac{1}{2}(\tilde{\alpha}_1 \ x) (\Sigma_H)^{-1} \begin{pmatrix} \tilde{\alpha}_1 \\ x \end{pmatrix}\right\}, \end{aligned} \quad (C3)$$

where

$$\tilde{\alpha}_1 = \sqrt{T} \text{Re } \alpha e^{-i\phi}, \quad \tilde{\alpha}_2 = \sqrt{T} \text{Im } \alpha e^{-i\phi}. \quad (C4)$$

The covariance matrix of the normal distribution (C3)

$$\Sigma_H = \begin{pmatrix} TV_A & 2TV_A \\ 2TV_A & 4TV_A + \sigma_x + \xi \end{pmatrix} \quad (C5)$$

gives the mutual information between Alice and Bob that can be computed from the formula [81]

$$I_{AB}^{(H)} = \frac{1}{2} \log \frac{\Sigma_{11}^H \Sigma_{22}^H}{\det \Sigma_H} = \frac{1}{2} \log \left[ 1 + \frac{4TV_A}{\sigma_x + \xi} \right], \quad (C6)$$

where  $\Sigma_{ii}^H$  are the diagonal elements of  $\Sigma_H$  and all logarithms are base 2.

Similarly, for double homodyne detection, from Eqs. (C2) and (49)) we have

$$\begin{aligned} p_B^{(DH)}(x, \tilde{\alpha}) &\propto \prod_{i=1}^2 \exp\left[-\frac{(x_i - \tilde{\alpha}_i)^2}{\sigma_i + \xi/2} - \frac{\tilde{\alpha}_i^2}{2TV_A}\right] \\ &= \prod_{i=1}^2 \exp\left\{-\frac{1}{2}(\tilde{\alpha}_i \ x_i) (\Sigma_{DH}^{(i)})^{-1} \begin{pmatrix} \tilde{\alpha}_i \\ x_i \end{pmatrix}\right\}. \end{aligned} \quad (C7)$$

Analogously to Eq. (C5), we obtain the diagonal blocks of the covariance matrix  $\Sigma_{DH}$  given by

$$\Sigma_{DH}^{(i)} = \begin{pmatrix} TV_A & TV_A \\ TV_A & TV_A + (2\sigma_i + \xi)/4 \end{pmatrix}, \quad i \in \{1, 2\}. \quad (C8)$$

Since  $p_B^{(DH)}(x, \tilde{\alpha}) = p_B^{(DH)}(x_1, \tilde{\alpha}_1)p_B^{(DH)}(x_2, \tilde{\alpha}_2)$ , the mutual information can be evaluated as a sum of two terms, determined by the above formula (C6) with  $\Sigma_H$  replaced by  $\Sigma_{DH}^{(i)}$ . The result reads

$$\begin{aligned} I_{AB}^{(DH)} &= \frac{1}{2} \sum_{i=1,2} \log \frac{[\Sigma_{DH}^{(i)}]_{11} [\Sigma_{DH}^{(i)}]_{22}}{\det \Sigma_{DH}^{(i)}} \\ &= \frac{1}{2} \sum_i \log \left[ 1 + \frac{4TV_A}{2\sigma_i + \xi} \right]. \end{aligned} \quad (C9)$$

In conclusion of this appendix, we briefly discuss equivalence relation between the prepare-and-measure (PM) and the entanglement-based (EB) schemes. To this end, we consider the two mode squeezed vacuum (TMSV) state given by [42]

$$|\Psi_{AB}\rangle = \frac{1}{\cosh r} \sum_{n=0}^{\infty} (\tanh r)^n |n, n\rangle_{AB}, \quad (C10)$$

where  $r$  is the real-valued squeezing parameter, with the covariance matrix [18]

$$\Sigma_{TMSV} = \begin{pmatrix} \cosh(2r)\mathbb{1} & \sinh(2r)\sigma_z \\ \sinh(2r)\sigma_z & \cosh(2r)\mathbb{1} \end{pmatrix}. \quad (C11)$$

In the EB protocol, Alice is assumed to hold the state  $\hat{\rho}_{AB} = |\Psi_{AB}\rangle\langle\Psi_{AB}|$ . Then Alice measures one mode using a noiseless double homodyne measurement, which corresponds to the coherent-state POVM (see Eq. (58))

$\{\hat{\Pi}_{CS}(\beta) = \pi^{-1}|\beta\rangle\langle\beta|\}_\beta$ , and sends the second mode to Bob. Unconditional state on the Bob's side prepared by such a measurement is

$$\hat{\rho}_B^{EB} = \int d^2\beta \text{Tr}_A\{(\hat{\Pi}_{CS}(\beta) \otimes \hat{I}_B)\hat{\rho}_{AB}\}. \quad (\text{C12})$$

By using the relation

$$\cosh r \langle \beta | \Psi_{AB} \rangle = \exp\left\{-\frac{|\beta|^2}{2 \cosh^2 r}\right\} |\tilde{\beta}\rangle, \quad (\text{C13})$$

where  $\tilde{\beta} = (\tanh r)\beta^*$ , the above density matrix (C12) can be recast into the form

$$\hat{\rho}_B^{EB} = \frac{1}{\pi \sinh^2 r} \int d^2\tilde{\beta} \exp\left\{-\frac{|\tilde{\beta}|^2}{\sinh^2 r}\right\} |\tilde{\beta}\rangle\langle\tilde{\beta}|. \quad (\text{C14})$$

When

$$\sinh^2 r = 2V_A \quad (\text{C15})$$

and  $\tilde{\beta}$  is changed to  $\alpha$ , the expressions for the input density matrix in the PM picture (79) and for the density matrix after Alice's measurement in the EB picture (C14) become identical. Since relation  $\cosh(2r) = 1 + 4V_A \equiv V$  immediately follows from Eq. (C15), the covariance matrix (C11) equals the matrix  $\Sigma_{TMSV}$  that enters Eq. (84). This results justify using the covariance matrix of TMSV for calculation of the Holevo information in the PM protocol.

---

[1] W. Vogel and D.-G. Welsch, *Quantum Optics*, 3rd ed. (Wiley-VCH, Berlin, 2006) p. 508.

[2] H. Yuen and J. Shapiro, Optical communication with two-photon coherent states—Part I: Quantum-state propagation and quantum-noise, *IEEE Transactions on Information Theory* **24**, 657 (1978).

[3] J. Shapiro, H. Yuen, and A. Mata, Optical communication with two-photon coherent states—Part II: Photoemissive detection and structured receiver performance, *IEEE Transactions on Information Theory* **25**, 179 (1979).

[4] H. Yuen and J. Shapiro, Optical communication with two-photon coherent states—Part III: Quantum measurements realizable with photoemissive detectors, *IEEE Transactions on Information Theory* **26**, 78 (1980).

[5] H. P. Yuen and V. W. S. Chan, Noise in homodyne and heterodyne detection, *Opt. Lett.* **8**, 177 (1983).

[6] N. G. Walker, Quantum theory of multiport optical homodyning, *Journal of Modern Optics* **34**, 15 (1987).

[7] M. J. Collett, R. Loudon, and C. W. Gardiner, Quantum theory of optical homodyne and heterodyne detection, *Journal of Modern Optics* **34**, 881 (1987).

[8] S. L. Braunstein, Homodyne statistics, *Phys. Rev. A* **42**, 474 (1990).

[9] W. Vogel and J. Grabow, Statistics of difference events in homodyne detection, *Phys. Rev. A* **47**, 4227 (1993).

[10] U. Leonhardt and H. Paul, Realistic optical homodyne measurements and quasiprobability distributions, *Phys. Rev. A* **48**, 4598 (1993).

[11] M. Ban, Quantum theory of the homodyne-direct receiver, *Journal of Modern Optics* **44**, 1175 (1997).

[12] K. Banaszek and K. Wódkiewicz, Operational theory of homodyne detection, *Phys. Rev. A* **55**, 3117 (1997).

[13] A. Kuzmich, D. Branning, L. Mandel, and I. A. Walmsley, Multiphoton interference effects at a beam splitter, *Journal of Modern Optics* **45**, 2233 (1998).

[14] S. Feng, D. He, and B. Xie, Quantum theory of phase-sensitive heterodyne detection, *J. Opt. Soc. Am. B* **33**, 1365 (2016).

[15] D.-G. Welsch, W. Vogel, and T. Opatrný, II Homodyne Detection and Quantum-State Reconstruction, in *Progress in Optics*, Vol. 39, edited by E. Wolf (Elsevier, Amsterdam, 1999) Chap. 2, pp. 63–211.

[16] G. Giedke and J. Ignacio Cirac, Characterization of Gaussian operations and distillation of Gaussian states, *Phys. Rev. A* **66**, 032316 (2002).

[17] J. Fiurášek and L. Mišta, Gaussian localizable entanglement, *Phys. Rev. A* **75**, 060302 (2007).

[18] A. Serafini, *Quantum Continuous Variables: A Primer of Theoretical Methods*, 2nd ed. (CRC Press, Taylor & Francis Group, Boca Raton, 2023) p. 362.

[19] W. Vogel, Homodyne correlation measurements with weak local oscillators, *Phys. Rev. A* **51**, 4160 (1995).

[20] A. Cives-Esclop, A. Luis, and L. L. Sánchez-Soto, An eight-port detector with a local oscillator of finite intensity, *Journal of Optics B: Quantum and Semiclassical Optics* **2**, 526 (2000).

[21] A. Auyuanet, E. Benech, H. Failache, and A. Lezama, Full statistics of ideal homodyne detection using real (noisy) local oscillator, *J. Opt. Soc. Am. B* **36**, 140 (2019).

[22] S. Olivares, A. Allevi, and M. Bondani, On the role of the local oscillator intensity in optical homodyne-like tomography, *Physics Letters A* **384**, 126354 (2020).

[23] G. S. Thekkadath, D. S. Phillips, J. F. F. Bulmer, W. R. Clements, A. Eckstein, B. A. Bell, J. Lugani, T. A. W. Wolterink, A. Lita, S. W. Nam, T. Gerrits, C. G. Wade, and I. A. Walmsley, Tuning between photon-number and quadrature measurements with weak-field homodyne detection, *Phys. Rev. A* **101**, 031801 (2020).

[24] U. Leonhardt, *Measuring the Quantum State of Light*, Cambridge Studies in Modern Optics (Cambridge University Press, Cambridge, 1997) p. 193.

[25] D. T. Smithey, M. Beck, M. G. Raymer, and A. Faridani, Measurement of the Wigner distribution and the density matrix of a light mode using optical homodyne tomography: Application to squeezed states and the vacuum, *Phys. Rev. Lett.* **70**, 1244 (1993).

[26] H. Kühn, D.-G. Welsch, and W. Vogel, Reconstruction of the quantum state of multimode light, *Phys. Rev. A* **51**, 4240 (1995).

[27] V. D'Auria, S. Fornaro, A. Porzio, S. Solimeno, S. Olivares, and M. G. A. Paris, Full characterization of gaus-

sian bipartite entangled states by a single homodyne detector, *Phys. Rev. Lett.* **102**, 020502 (2009).

[28] A. I. Lvovsky and M. G. Raymer, Continuous-variable optical quantum-state tomography, *Rev. Mod. Phys.* **81**, 299 (2009).

[29] D. Buono, G. Nocerino, V. D'Auria, A. Porzio, S. Olivares, and M. G. A. Paris, Quantum characterization of bipartite Gaussian states, *J. Opt. Soc. Am. B* **27**, A110 (2010).

[30] Y. S. Teo, C. R. Müller, H. Jeong, Z. Hradil, J. Řeháček, and L. L. Sánchez-Soto, Superiority of heterodyning over homodyning: An assessment with quadrature moments, *Phys. Rev. A* **95**, 042322 (2017).

[31] E. S. Tiunov, V. V. T. (Vyborova), A. E. Ulanov, A. I. Lvovsky, and A. K. Fedorov, Experimental quantum homodyne tomography via machine learning, *Optica* **7**, 448 (2020).

[32] S. Olivares, A. Allevi, G. Caiazzo, M. G. A. Paris, and M. Bondani, Quantum tomography of light states by photon-number-resolving detectors, *New Journal of Physics* **21**, 103045 (2019).

[33] B. Qi, P. Lougovski, and B. P. Williams, Characterizing photon number statistics using conjugate optical homodyne detection, *Opt. Express* **28**, 2276 (2020).

[34] C. Kumar and Arvind, Estimation of the Wigner distribution of single-mode Gaussian states: A comparative study, *Phys. Rev. A* **105**, 042419 (2022).

[35] C. Oh, C. Lee, C. Rockstuhl, H. Jeong, J. Kim, H. Nha, and S.-Y. Lee, Optimal Gaussian measurements for phase estimation in single-mode Gaussian metrology, *npj Quantum Information* **5**, 10 (2019).

[36] S. L. Braunstein and P. van Loock, Quantum information with continuous variables, *Rev. Mod. Phys.* **77**, 513 (2005).

[37] A. A. Semenov, F. Töppel, D. Y. Vasylyev, H. V. Gomonay, and W. Vogel, Homodyne detection for atmosphere channels, *Phys. Rev. A* **85**, 013826 (2012).

[38] A. Furusawa, J. L. Sørensen, S. L. Braunstein, C. A. Fuchs, H. J. Kimble, and E. S. Polzik, Unconditional quantum teleportation, *Science* **282**, 706 (1998).

[39] S. Shi, Y. Wang, L. Tian, W. Li, Y. Wu, Q. Wang, Y. Zheng, and K. Peng, Continuous variable quantum teleportation network, *Laser & Photonics Reviews* **17**, 2200508 (2023).

[40] F. Grosshans and P. Grangier, Continuous variable quantum cryptography using coherent states, *Phys. Rev. Lett.* **88**, 057902 (2002).

[41] C. Weedbrook, A. M. Lance, W. P. Bowen, T. Symul, T. C. Ralph, and P. K. Lam, Quantum cryptography without switching, *Phys. Rev. Lett.* **93**, 170504 (2004).

[42] C. Weedbrook, S. Pirandola, R. García-Patrón, N. J. Cerf, T. C. Ralph, J. H. Shapiro, and S. Lloyd, Gaussian quantum information, *Rev. Mod. Phys.* **84**, 621 (2012).

[43] Y. Zhang, Y. Bian, Z. Li, S. Yu, and H. Guo, Continuous-variable quantum key distribution system: Past, present, and future, *Applied Physics Reviews* **11**, 011318 (2024).

[44] V. Scarani, H. Bechmann-Pasquinucci, N. J. Cerf, M. Dušek, N. Lütkenhaus, and M. Peev, The security of practical quantum key distribution, *Rev. Mod. Phys.* **81**, 1301 (2009).

[45] F. Xu, X. Ma, Q. Zhang, H.-K. Lo, and J.-W. Pan, Secure quantum key distribution with realistic devices, *Rev. Mod. Phys.* **92**, 025002 (2020).

[46] Y.-M. Chi, B. Qi, W. Zhu, L. Qian, H.-K. Lo, S.-H. Youn, A. I. Lvovsky, and L. Tian, A balanced homodyne detector for high-rate Gaussian-modulated coherent-state quantum key distribution, *New Journal of Physics* **13**, 013003 (2011).

[47] P. Jouguet, S. Kunz-Jacques, E. Diamanti, and A. Leverrier, Analysis of imperfections in practical continuous-variable quantum key distribution, *Phys. Rev. A* **86**, 032309 (2012).

[48] S. Wang, P. Huang, T. Wang, and G. Zeng, Feasibility of all-day quantum communication with coherent detection, *Phys. Rev. Applied* **12**, 024041 (2019).

[49] C. Lupo and Y. Ouyang, Quantum key distribution with nonideal heterodyne detection: Composable security of discrete-modulation continuous-variable protocols, *PRX Quantum* **3**, 010341 (2022).

[50] A. A. Semenov, J. Samelin, C. Boldt, M. Schünemann, C. Reiher, W. Vogel, and B. Hage, Photocounting measurements with dead time and afterpulses in the continuous-wave regime, *Phys. Rev. A* **109**, 013701 (2024).

[51] A. A. Hajomer, A. N. Oruganti, I. Derkach, U. L. Andersen, V. C. Usenko, and T. Gehring, Finite-size security of continuous-variable quantum key distribution with imperfect heterodyne measurement, *arXiv preprint arXiv:2501.10278* (2025).

[52] A. n. Oruganti, I. Derkach, R. Filip, and V. C. Usenko, Continuous-variable quantum key distribution with noisy squeezed states, *Quantum Science and Technology* **10**, 025023 (2025).

[53] J.-Z. Huang, Z.-Q. Yin, S. Wang, H.-W. Li, W. Chen, G.-C. Guo, and Z.-F. Han, Wavelength attack scheme on continuous-variable quantum key distribution system using heterodyne detection protocol, *arXiv preprint arXiv:1206.6550* (2012).

[54] J.-Z. Huang, S. Kunz-Jacques, P. Jouguet, C. Weedbrook, Z.-Q. Yin, S. Wang, W. Chen, G.-C. Guo, and Z.-F. Han, Quantum hacking on quantum key distribution using homodyne detection, *Physical Review A* **89**, 032304 (2014).

[55] H. Qin, R. Kumar, V. Makarov, and R. Alléaume, Homodyne-detector-blinding attack in continuous-variable quantum key distribution, *Physical Review A* **98**, 012312 (2018).

[56] H. Qin, R. Kumar, and R. Alléaume, Quantum hacking: Saturation attack on practical continuous-variable quantum key distribution, *Physical Review A* **94**, 012325 (2016).

[57] M. Zou, Y. Mao, and T.-Y. Chen, Rigorous calibration of homodyne detection efficiency for continuous-variable quantum key distribution, *Opt. Express* **30**, 22788 (2022).

[58] X.-Y. Wang, X.-B. Guo, Y.-X. Jia, Y. Zhang, Z.-G. Lu, J.-Q. Liu, and Y.-M. Li, Accurate shot-noise-limited calibration of a time-domain balanced homodyne detector for continuous-variable quantum key distribution, *J. Lightwave Technol.* **41**, 5518 (2023).

[59] S. Pan, D. Monokandylos, and B. Qi, Detector noise in continuous-variable quantum key distribution, *Physical Review A* **112**, 10.1103/4h84-5tsg (2025).

[60] A. Barchielli and A. Santamato, Eight-port homodyne detector: The effect of imperfections on quantum random-number generation and on detection of quadratures, *Phys. Rev. A* **106**, 022620 (2022).

[61] A. Ruiz-Chamorro, D. Cano, A. García-Callejo, and

V. Fernandez, Effects of experimental impairments on the security of continuous-variable quantum key distribution, *Heliyon* **9**, e16670 (2023).

[62] J. O. Bartlett, A. J. M. Wilson, C. J. Chunnilall, and R. Kumar, Detector asymmetry in continuous variable quantum key distribution, arXiv preprint arXiv:2510.17419 (2025).

[63] P. L. Kelley and W. H. Kleiner, Theory of electromagnetic field measurement and photoelectron counting, *Phys. Rev.* **136**, A316 (1964).

[64] J. G. Skellam, The frequency distribution of the difference between two Poisson variates belonging to different populations, *Journal of the Royal Statistical Society Series A: Statistics in Society* **109**, 296 (1946).

[65] F. W. J. Olver, D. W. Lozier, R. F. Boisvert, and C. W. Clark, eds., *NIST Handbook of Mathematical Functions* (NIST & Cambridge University Press, New York, 2010) p. 951.

[66] P. Lahti, J.-P. Pellonpää, and J. Schultz, Realistic eight-port homodyne detection and covariant phase space observables, *Journal of Modern Optics* **57**, 1171 (2010).

[67] T. Richter, Double homodyne detection and quantum state determination, in *European Quantum Electronics Conference* (Optica Publishing Group, 1998) p. QTUG38.

[68] C. Weedbrook, A. M. Lance, W. P. Bowen, T. Symul, T. C. Ralph, and P. K. Lam, Quantum cryptography without switching, *Phys. Rev. Lett.* **93**, 170504 (2004).

[69] A. Leverrier, Security of continuous-variable quantum key distribution via a gaussian de finetti reduction, *Phys. Rev. Lett.* **118**, 200501 (2017).

[70] M. G. Genoni, S. Mancini, and A. Serafini, General-dyne unravelling of a thermal master equation, *Russian Journal of Mathematical Physics* **21**, 329 (2014).

[71] F. Grosshans and P. Grangier, Continuous variable quantum cryptography using coherent states, *Phys. Rev. Lett.* **88**, 057902 (2002).

[72] F. Laudenbach, C. Pacher, C.-H. F. Fung, A. Poppe, M. Peev, B. Schrenk, M. Hentschel, P. Walther, and H. Hübel, Continuous-variable quantum key distribution with Gaussian modulation—the theory of practical implementations, *Advanced Quantum Technologies* **1**, 1800011 (2018).

[73] I. Devetak and A. Winter, Distillation of secret key and entanglement from quantum states, *Proceedings of the Royal Society A: Mathematical, Physical and Engineering Sciences* **461**, 207 (2005).

[74] M. Navascués, F. Grosshans, and A. Acín, Optimality of Gaussian attacks in continuous-variable quantum cryptography, *Phys. Rev. Lett.* **97**, 190502 (2006).

[75] R. García-Patrón and N. J. Cerf, Unconditional optimality of Gaussian attacks against continuous-variable quantum key distribution, *Phys. Rev. Lett.* **97**, 190503 (2006).

[76] A. Ruiz-Chamorro, D. Cano, A. García-Callejo, and V. Fernandez, Effects of experimental impairments on the security of continuous-variable quantum key distribution, *Heliyon* **9** (2023).

[77] J. Lodewyck, M. Bloch, R. García-Patrón, S. Fossier, E. Karpov, E. Diamanti, T. Debuisschert, N. J. Cerf, R. Tualle-Brouri, S. W. McLaughlin, and P. Grangier, Quantum key distribution over 25 km with an all-fiber continuous-variable system, *Phys. Rev. A* **76**, 042305 (2007).

[78] V. C. Usenko and R. Filip, Trusted noise in continuous-variable quantum key distribution: A threat and a defense, *Entropy* **18**, 10.3390/e18010020 (2016).

[79] F. Laudenbach and C. Pacher, Analysis of the trusted-device scenario in continuous-variable quantum key distribution, *Advanced Quantum Technologies* **2**, 1900055 (2019).

[80] M. Freyberger, K. Vogel, and W. P. Schleich, From photon counts to quantum phase, *Physics Letters A* **176**, 41 (1993).

[81] J. Soch *et al.*, Statproofbook/statproofbook.github.io: The book of statistical proofs (version 2023), <https://doi.org/10.5281/zenodo.4305949> (2024), accessed: 2025-07-15.